Addis Ababa University
Institute of Technology
School of Mechanical and Industrial Engineering

# Effect of Change of Rail Profile on Rolling Contact Fatigue at Wheel-Rail Interface

**A master's thesis submitted to the school of mechanical and industrial of Addis Ababa University in partial fulfillment of the requirements for the degree of Master of Science in mechanical engineering under railway program.**

**Submitted by:**

**Teklebrhan Abebe GSR /3239/06 E.C**

**Submitted to:**

**Dr. Daniel Tilahun**

**June 19, 2017 Addis Ababa, Ethiopia**

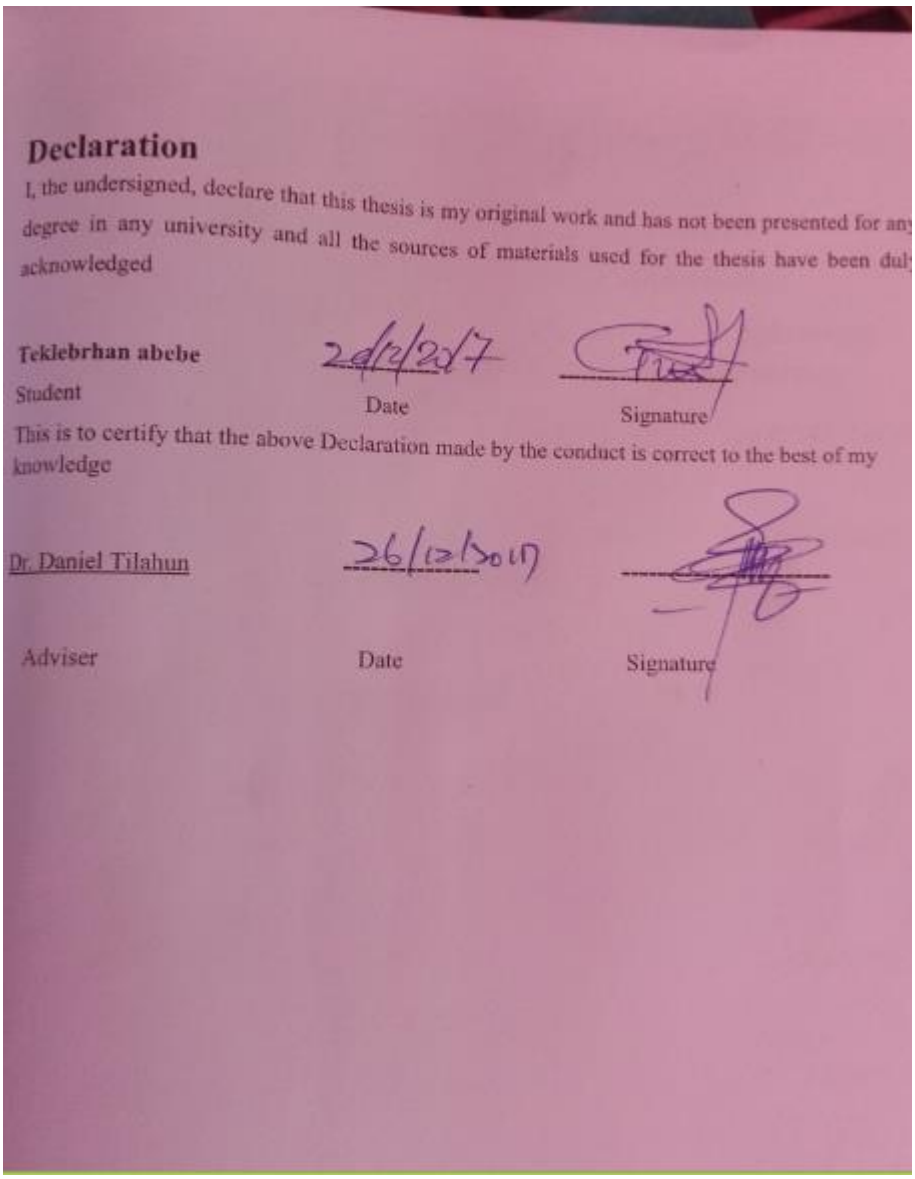

**Declaration**

I, the undersigned, declare that this thesis is my original work and has not been presented for any degree in any university and all the sources of materials used for the thesis have been duly acknowledged

**Teklebrhan abebe** 2/12/2017

Student Date Signature

This is to certify that the above Declaration made by the conduct is correct to the best of my knowledge

Dr. Daniel Tilahun 26/12/2017

Adviser Date Signature

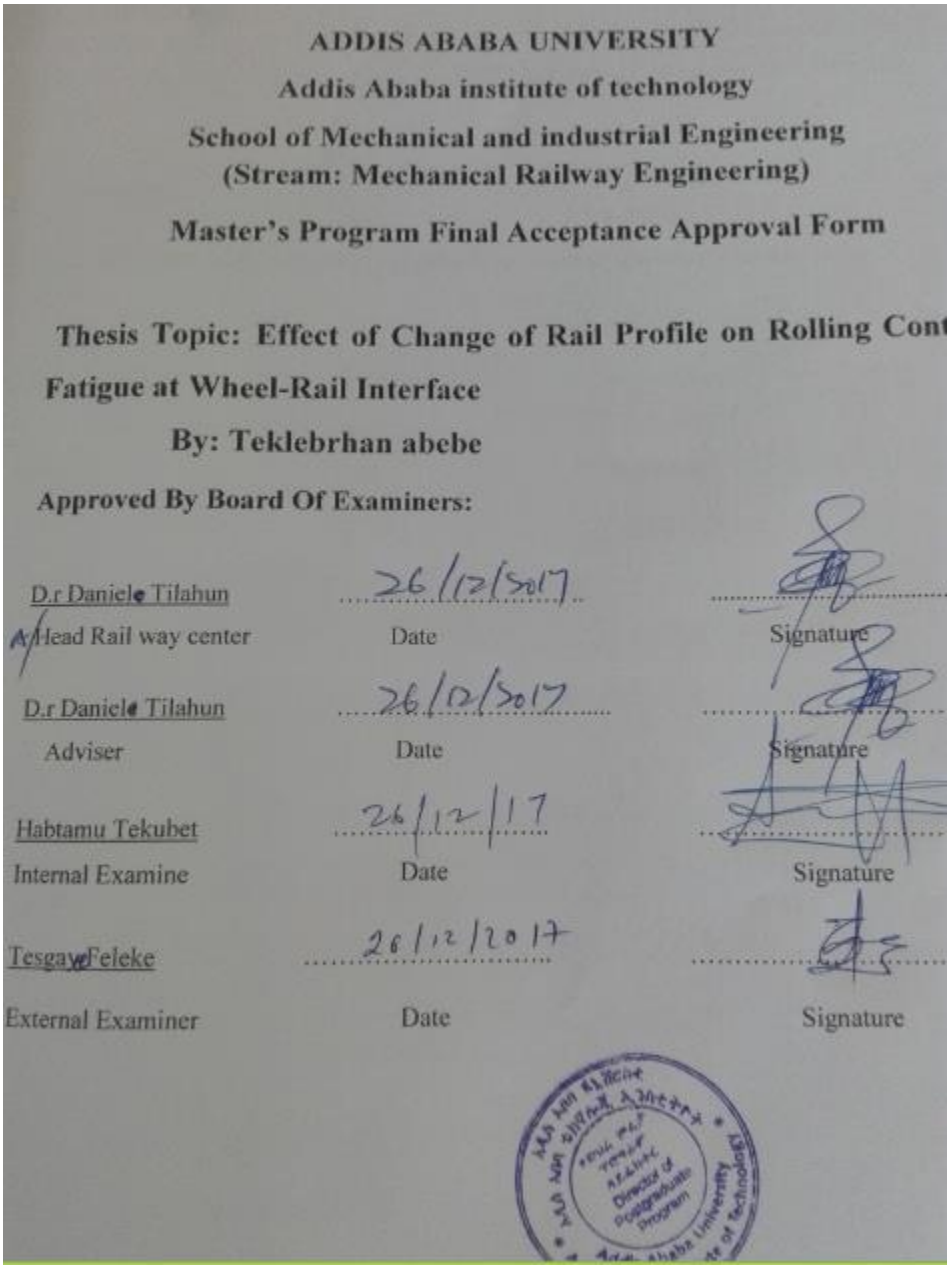

ADDIS ABABA UNIVERSITY

Addis Ababa institute of technology

School of Mechanical and industrial Engineering

(Stream: Mechanical Railway Engineering)

Master's Program Final Acceptance Approval Form

Thesis Topic: Effect of Change of Rail Profile on Rolling Cont

Fatigue at Wheel-Rail Interface

By: Teklebrhan abebe

Approved By Board Of Examiners:

| | | | |
|---|---|---|---|
| D.r Daniele Tilahun<br>Head Rail way center | 26/12/2017 | Date | Signature |
| D.r Daniele Tilahun<br>Adviser | 26/12/2017 | Date | Signature |
| Habtamu Tekubet<br>Internal Examine | 26/12/17 | Date | Signature |
| Tesgaye Feleke<br>External Examiner | 26/12/2017 | Date | Signature |

## Acknowledgments

First of all, I would like to thank my advisor Dr. Daniel Tuliahan for his grateful support and continuous advice of the work from the beginning up to the final result of this paper. I want to appreciate also his willingness and giving of motivations to work on research areas focusing on the current situations of our country, Ethiopia, pointing its future development and related problems to lay down the possible respective solutions.

I would like to thank Ethiopian Railway Corporation, for giving me a chance to study this degree and who covers the entire school fee and paying me the pocket money the past two years. Their willingness to produce skilled manpower for the future expansion of Ethiopian Railway is highly appreciated.

Finally, special thanks to my Family and friends for their patience, advice, support and motivation standing always on my side for the successful accomplishment of this paper and for the success of my girlfriends at all.

# Effect of change of Rail profile on Rolling Contact Fatigue stress at Wheel-Rail Interface


## Abstract

The general objective of this thesis is to analyze effect of change of radiuses curvature of Rail profile on contact fatigue stress using analytic and finite element software's. The formulation in this study aims primarily at determination of stresses and fatigue parameters by varying contact area arising from variation in radiuses curvature of Rail profile. A change in radiuses curvature of Rail profile brings in a change in contact area and stresses. The theoretical models are based on the normal problem (Hertz theory) correspondingly, variations in the results in terms of principal stresses and fatigue parameters such as equivalent stresses, fatigue damage, and expected fatigue life with changes in radiuses curvature of Rail profile are obtained. Comparisons of different radiuses curvature of Rail profile are taken place. Better radiuses curvature of Rail profile is suggested. Results obtained are expected to help understand the rail wheel configuration dependence on the stress deformation pattern and fatigue parameters. This may help an appropriate selection of radiuses curvature of Rail profile in the optimization process.

# Effect of change of Rail profile on Rolling Contact Fatigue stress at Wheel-Rail Interface

## Contents

**List of Figures**

## List of tables

## List of symbols

| | |
|---|---|
| *a* | Major axes of the hertizian contact patch |
| *b* | Minor axes of the hertizian contact patch |
| $Fz_{=FN}$ | the normal force |
| F x | Longitudinal creep force |
| ξ | longitudinal creep age |
| F y | Lateral creep force |
| η | lateral creep |
| Po | The maximum contact stress |
| P(x y) | the pressure distribution within the contact ellipse |
| $\sigma_x$ | The principal stresses along the x axes at or below, the contact center |
| $\sigma_y$ | The principal stresses along the y axes at or below, the contact center |
| $\sigma_z$ | The principal stresses acting the z axes at or below, the contact center |
| $R_{11}$ = r: | The rolling radius of curvature of the wheel. |
| $R_{12}$=ρr | the radius of wheel profile, which goes to infinity for a conical wheel. |
| $R_{21}$: | The radius of the runway which is infinity in this case. |
| $R_{22}$=ρs | The radius of curvature of the rail in the plane of cross section. |
| Y | The yield stress in simple tension |
| σh | The hydrostatic stress |
| $\tau_{max}$ | The maximum principal shear stress |
| τa | The shear stress amplitude |
| τe | The fatigue limit in alternating shear |
| σe | The fatigue limit in rotating bending |
| ȧDV | The Dang Van material parameter |
| σu | The tensile fracture stress of the material |
| $\sigma_{EQ}$ | Equivalent stress |
| Fp | Fatigue parameter |
| Δε | The range of the normal strain |
| Δϑ | The range of the (engineering) shear strain |

| | |
|---|---|
| $\Delta\tau$ | The range of the shear stress |
| $\tau_1$ | The maximum principal shear stress in the plane of deformation |
| E | Young's elasticity modulus |
| $\epsilon'_f$ | Additional material parameter |
| *b* | Additional material parameter |
| c | Additional material parameter |
| *J* | material parameter |
| K | The yield stress in simple shear |
| εi | The current strain increment |
| εc | The fracture strain |
| $\delta_{ut}$ | Ultimate tensile strength |
| $\sigma'_f$ | Fatigue strength coefficient |
| n or m | Paris Exponent of the material |
| A and B | wheel-rail geometric configuration |
| $K_1$ and $K_2$ | that depend on the material properties |
| *f* | The traction coefficient |
| qo | traction force |
| D | fatigue damage |
| N*f* | Expected fatigue life. |
| *W* | Wear index |

# Chapter One

## 1.1. Introduction

In the wheel-rail contact area both rolling and sliding may occur. The radius curvature of wheel-rail at the contact area would be change after quite a long time in service due to sliding of wheel on the rail. In order to investigate the influence of the change radius curvature of rail profile on the shape of the contact zone and contact fatigue stress.

The wheel-rail contact and size of the forces transmitted into contact zone influence various damage mechanisms like, wear and surface cracking. The wheel load is transmitted to the rail through a tiny contact area under high contact stress. This results in repeated loading above the elastic limit which leads to plastic deformation. The depth of plastic flow depends on the hardness of the rail and the severity of the curves.

The nature of the fit between contacting bodies is divided into two types namely conformal and non-conformal. Conformal contact occurs where the surfaces contact uniformly over their contacting boundaries resulting in a large contact area in relation to the size of the contacting objects. This contact generates a stress field which propagates uniformly throughout the bodies and is tied to the general stress field of the bulk of the bodies Non-conformal contact on the other hand begins in the form of point or line contact which develops with increasing loading into a contact patch with a small contact area in relation to the size of the contacting bodies. In general cases this patch is of an elliptical shape and depends on the orthogonal radii of curvature at the contact point of the contacting bodies. This result in local stress concentrations and stresses in the region of contact much greater than the general stresses in the bulk of the bodies The case of railway wheel/rail interaction falls into the non-conformal category with two possible contact regions being present. The wheel-tread/rail-head contact is always present and results in the development of a contact patch those changes in shape with the loading conditions and the transverse location of the wheel on the rail. It is the dominant contact for drive traction, braking and self-steering. The wheel-flange/rail-head contact is not always present and forms the hard limit for the motion of the wheel for linear movement transverse to the rail as well as for angular

misalignment of the axle. This patch has the dominant role in extreme hunting phenomenon and train steering.

In railway infrastructure in order to increase the speed of trains, to increase the axles loads of trains and locomotives traction, to increase the density of traffic and to increase resistance to harmful influences of the environment (environmental aspects), requires improved quality of rails. Rails as an important part of the railway infrastructure have exact level of quality. In Europe, the quality of rails is prescribed by international standards, the European Union of Railways UIC 860 and EN13674. [Bratislava Sladojevic, 2010]

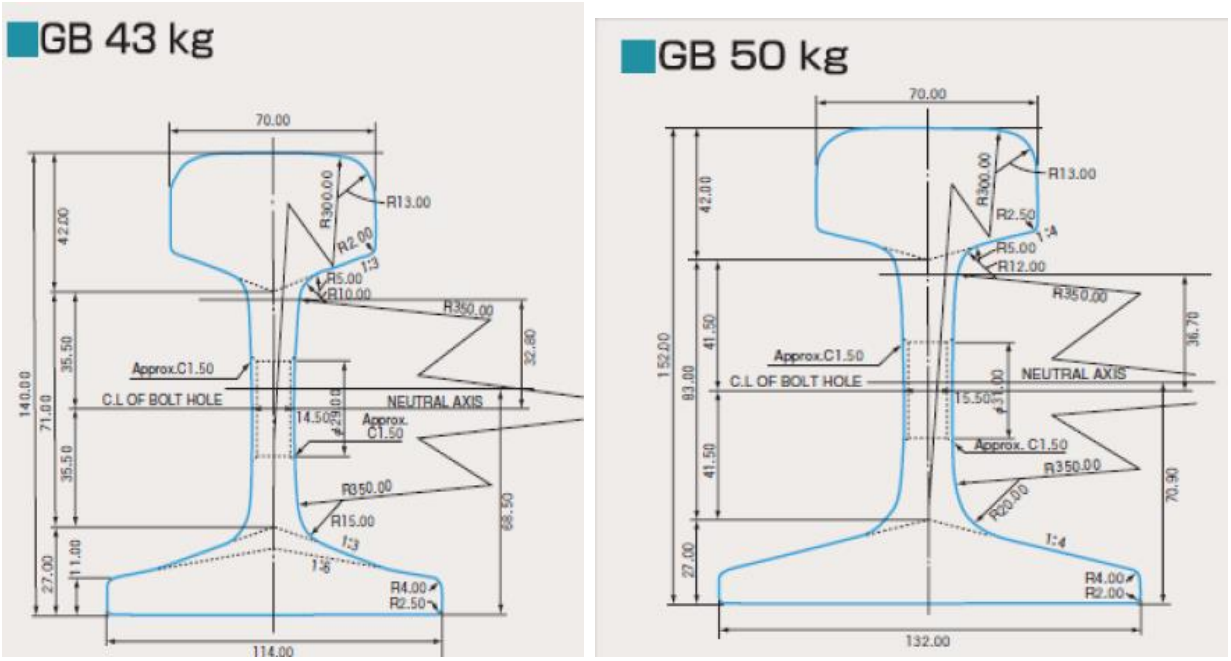


**Figure 1.1**: Typical Chinese standard rails

### 1.1.1Railway-wheel

A railway wheel, together with an axle, is one of the fundamental parts that support the safe operation of railway vehicles. Wheels support the entire weight of cars; however, they cannot be designed as a failsafe structure where a backup system by other parts can be applied in case of a serious problem. Therefore, absolutely high reliability is demanded in terms of strength. Accordingly, the most important and fundamental characteristic in designing wheels is strength.

A solid wheel of a railway vehicle consists of three parts, as shown in Fig. 1.2. They include:

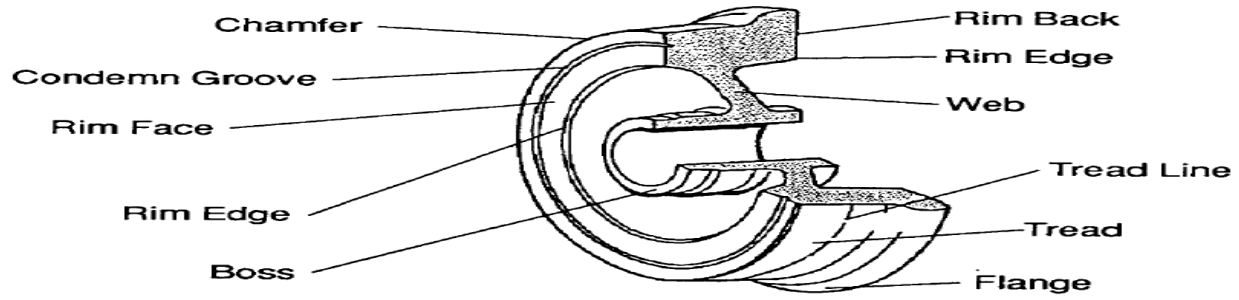


Figure1.2 Parts of a solid wheel

**Hub**: wherein an axle is inserted

**Rim**: part that contacts the rail

**Web**: part that unites the two parts (hub and rim).

**Tread:** the outer circumferential surface of the rim, which contacts the rail and

**Flange:** the projected part of the rim.

The initiation of subsurface cracks requires very high load levels, introduced by type of loads due to track geometry [15]. Like surface cracks, subsurface-induced cracks will also propagate parallel, or in an inclined angle to the wheel surface. At a certain point they may, however, branch towards the surface [14] and/or in radial direction [16]. The second alternative includes the danger of catastrophic failure. Subsurface-induced failures are potentially more dangerous than surface-induced because of a larger crack extension before spelling all forms of metal failure associated with repeated contact stress cycles are usually called rolling contact fatigue

## 1.1.2 Railway-Rails

Rails are longitudinal members made by steel that are placed on spaced sleepers to guide the rolling stock. Their strength and stiffness must be sufficient to maintain a steady shape and smooth track configuration, and resist various forces by vehicles. The principal function of the rail is to accommodate and transfer the wheel loads onto the supporting sleepers.

Rails are one of the railway system components arranged in parallel to provide a continuous and level surface for train movement, provide lateral guidance to the train wheels, bear the wheel load.

All modern railways use steel rails which are specifically rolled for the purpose from steel which has the required qualities of strength, fatigue endurance and wear and corrosion resistance.

The shape of the rail has now become generally standardized as the Flat Bottom (FB) rail. The head of the rail has an almost flat top with curves at the outer edges designed to fit the shape of the wheel tire. One of the features of a well matched rail head and wheel tire is that, when the axis of the wheel coincides with the longitudinal axis of the track and the rail is set at its correct inclination of 1 in 20 to the vertical, the point of contact between the two is very close to the center line of the rail. This is very desirable since it minimizes the twisting effect on the rail which a concentrically applied wheel load would produce, and by keeping the contact area away from the gauge corner, reduces both corner 'shelling' and fatigue damage.

The rail head sides slope is at 1 in 20. This is to compensate for the 1 in 20 inwards slopes of the rails and not only makes it simpler to check the gauge but ensures that when side wear takes place the associated gauge widening is minimized.

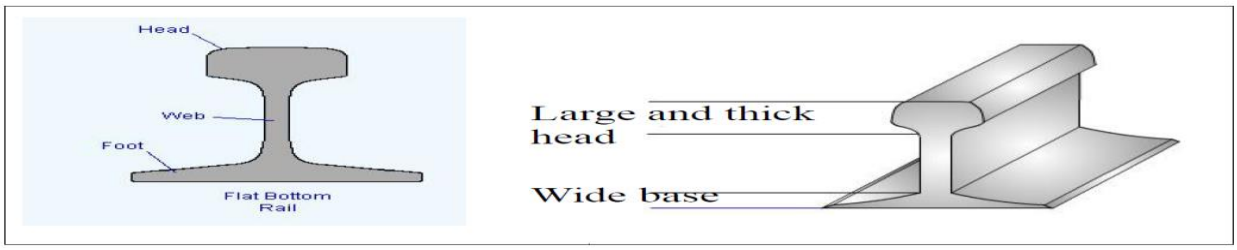


Figure1.3: Rail profile

### 1.1.3 Wheel and Rail profile

The main aim of the wheel and rail profile design is to provide a wheel guidance tool. However, these profiles play an important role in determining the magnitude and distribution of the wheel-rail contact stresses. In service both the profiles change continuously, due to wear, rail grinding and wheel re profiling. More conformal profiles, caused by wear, results in larger contact area, and as a result, lower contact stresses. In the contrary rail grinding and wheel re profiling results in a less conformal contact and higher stresses. Recently, reduction of contact stresses started to play an important role in the design of wheel and rail profiles. Munich suggested different actions to extend the rail life among which is the introduction of new wheel profiles. Greg and Singer studied

the effect of wheel iconicity on the flange force and showed that this force increases with the iconicity angle of the wheel. Di Briton et al have studied the important role of wheel and rail profiles in creating contact geometries that adversely affect wheel set steering.

### 1.1.4 Rolling contact fatigue (RCF)

Rolling contact fatigue (RCF) of rails is a term used to describe fatigue failures caused by the wheel/rail contact stresses. The initiation of RCF cracks, which can either be surface or subsurface, appears to be similar to that of delimitation wear in rails, these cracks is characterized by a main crack propagating in the forward direction with respect to traffic. They branch downwards at a depth of 3-4 mm below the surface to produce transverse defect such a defect caused by a subsurface initiated RCF crack other fatigue failures.

#### 1.1.4.1 Rolling contact fatigue in Rail

Numerous terms are used to describe the different types of rail fatigue cracking in different areas of the world. The type of cracking also varies with the different rail grades, traffic types, vehicle characteristics and maintenance regimes. The main categories of railhead fatigue failure are 'head checks', 'squats' and 'tongue is lapping', as shown in Figure 1.4. The broad characteristics included in these failures are explained below.

- ✓ Head Checks: When occurring at the gauge corner, it is referred to as 'gauge corner cracking'. They are initiated as small fine cracks on the rail surface which grow down into the rail at a shallow angle below the surface. As they grow with time, they either branch down causing the rail to break, or branch up leading to spelling of the rail surface.

- ✓ Squats: Identified by a darkening of the rail surface, combined with widening of the running band. This phenomenon is due to a horizontal crack below the surface which allows the near surface material to flow sideways, thereby producing widening of the running band, often combined with a surface depression which collects dirt and becomes corroded, leading to the characteristic shadowing. Branch cracks can form from the original horizontal crack, leading to spelling of the rail surface, or rail breakage.
- ✓ Tongue lapping: Identified by the removing of thin slivers or tongues of material from the running band of the rail, frequently extending down the gauge face of the rail by several

millimeters. Cracks can form below the extruded steel and grow into the railhead in a near horizontal plane can then form, running either up or down, leading to rail breakage.

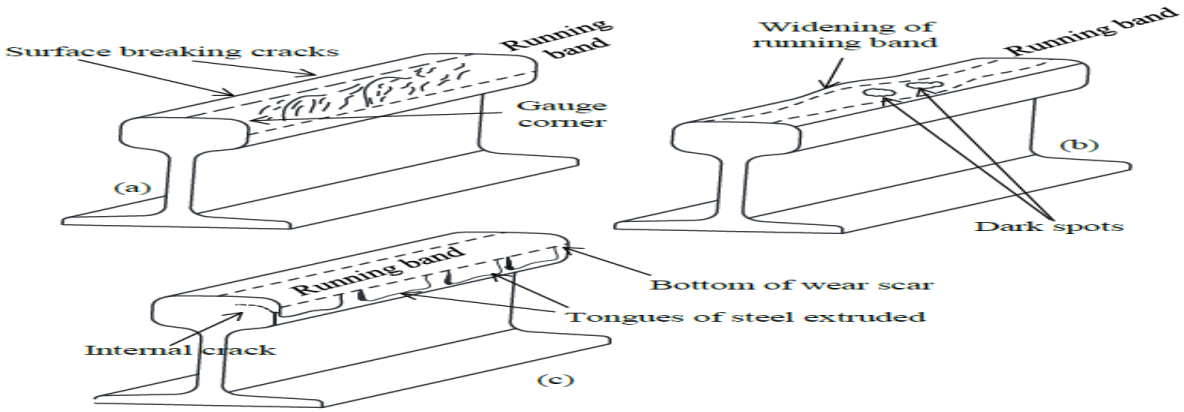


**Figure1.4:** Schematic illustrations of common rail fatigue damage types: (a) head checks; (b) squats; (c) tongue lapping (Adapted from

### 1.1.4.2 Wheel rolling contact fatigue (RCF)

Damage accumulation due to fatigue, plastic deformation and wear, significantly reduces the service life of the railway track [7]. In recent years, higher train speeds and increased axle loads have led to larger wheel/rail contact forces. Also, efforts have been made to optimize wheel and rail design. This evolution tends to change the major wheel rim damage from wear to fatigue [7]. Unlike the slow deterioration process of wear, fatigue causes abrupt fractures in wheels or the tread surface material loss. These failures may cause damage to rails, damage to train suspensions and, in rare cases, serious derailment of the train. The fatigue problem of railroad wheels is often referred to as rolling contact fatigue [30], which is caused by repeated contact stress during the rolling motion. The proper understanding of the underlying mechanism of rolling contact fatigue requires detailed knowledge of the interaction between wheel and rail. A proper multi axial fatigue damage accumulation model under rolling contact stress state is required.

Railroad wheels may fail in different ways corresponding to different failure mechanisms Ekberg A, Marais the wheel fatigue failure modes into three different failure types corresponding to different initiation locations. Surface initiated, subsurface initiated and deep surface initiated fatigue failures. On the tread surface, there are usually two types of cracks. One is caused by the repeated mechanical contact stress. The other is initiated by thermal stresses arising from on-tread

friction braking. But, this thesis focuses on rolling contact fatigue damage due to repeated mechanical contact stress.

Surface initiated fatigue: initiation of surface cracks is related to plastic deformation of the material in the surface layer of the wheel rim. The main cause of global plastic deformation of the surface material is the applied interfacial shear stress between the wheel tread and the rail head. Surface initiated RCF cracks are more common, but less severe than sub surface initiated RCF cracks on a wheel fleet. The loading is likely to be lower than what is optimum from an economical point of view. Still, this is a delicate balance. When the loading (in a broad sense) is increased above a certain level, an epidemic of surface initiated cracks will occur with cracking frequencies and severity exceeding acceptable levels.

### 1.1.5 Wheel loads

Normal contact stress is a function of four main factors; wheel diameter, wheel load (including possible dynamic loading), the transverse rail profile and the transverse profile of the wheel. According to Hertz ‘s elastic contact equations, the doubling of wheel load will increase contact stress. If, with respect to the strength of the material and traction coefficient, this increase is sufficient to place the material beyond the fatigue boundaries, then the consequences are indeed dire. Although the nominal static wheel loads are generally set by commercial concerns and limits on track infrastructure (often bridges), management of dynamic loads has the potential to reduce dramatically the incidents of broken rails broken wheels and wheel shelling in particular. Dynamic wheel loading associated with flat spots or out-of-round wheels, poorly straightened and aligned rail, insufficient tie support, rail and wheel corrugation, dipped welds, poorly maintained turnouts, etc., can be detected and managed. Uneven loading, poor can’t selection and poor truck/bogie wheel load equalization capabilities are further contributors to wheel and rail damage. As noted in the reduction of dynamic loads and more even spreading of stress is an approach to either limiting rail damage or allowing for greater static wheel loads

### 1.1.6 Track geometry

The geometrical parameters of the track play an important role in the deterioration caused by the wheel-rail contact. The main geometrical parameter in this regard is the wheel and rail profiles and

the position of the rail in relation to the curve incurved tracks. Smallwood have shown that the maximum contact stress on the rails dictated by the lateral wheel set shift. Using a vehicle dynamic software package they concluded that the maximum contact pressure on the outer (high) rail is more than that on the inner rail. The situation is more aggravated by the direction of the creep age force, caused by steering forces which has been found to oppose the load movement direction on the outer rail and match it on the inner rail. This may explain the reason behind the outer rail being more prone to rolling contact fatigue failure which favors traction opposite to the load movement. The arrows on the diagram indicate the direction and magnitude of the contact forces is a prediction of the maximum contact stress due to leading Wheel set

### 1.1.7 Cyclic loading

In wheel-rail contact, the loading takes the form of repeated cycles. The response of material to cyclic loading, in this case, can take four different forms, as listed below and illustrated in figure Perfectly elastic behavior if the load does not exceed the elastic limit during any load cycle, Elastic shakedown, where plastic deformation takes place during the early cycles but, due to the development of residual stresses and the strain hardening of some materials, such as steel, the steady state behavior is perfectly elastic, see figure (1.4b). The load below which this is possible is referred to as the elastic shakedown limit Plastic shakedown, in which the steady state is a closed elastic-plastic loop but with no net accumulation of plastic deformation. This behavior is sometimes referred to as cyclic plasticity, figure (1.4c), and the corresponding load limit is called the plastic shakedown limit or the ratcheting threshold. Above the ratcheting threshold, the steady state consists of an open elastic-plastic loops and the material accumulates a net unidirectional strain during each cycle, a process known as ratcheting; shown in figure Ratcheting is sometimes referred to as incremental collapse. Recently, this type of analysis has received great attention and has been employed to explain the wear behavior of different materials a shakedown map as a function of contact pressure, coefficient of fiction and the shear yield strength of the material This subject will be discussed.

### 1.1.8 Axial loads

An operated on one track Defects in the running surface of the rails such as joints, dips and twists and irregularities in the wheel such as Flats and out of roundness may play a role. Axial stresses arise from structural irregularities of the track and from the acceleration and deceleration of the train during train start and stop. The Loading due to rolling contact is similar to what has been discussed for wheels and plays a major role in the early crack extension phase. Note, that there is additional loading in lateral direction especially in curved track sections and at switches and crossovers. These forces are also dynamically magnified with increasing speed. For trains equipped with tilting technology local track irregularities in particular in small-radius curves seem to play a major role with respect of lateral load increase in track and boggy as well [23]. The main load case for rails in switches is horizontal lateral bending.

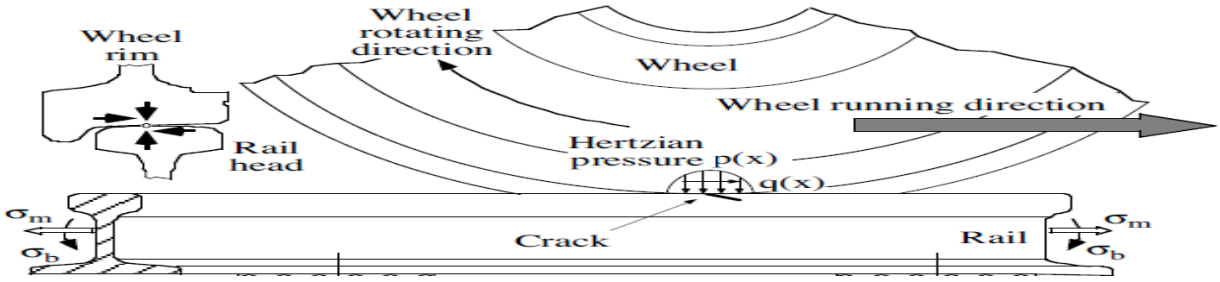


**Figure1.5:** Primary loading configuration of a rail

The primary loads are superimposed by secondary loads, which, by their nature, are thermal and residual stresses. A rail track is installed at a certain ambient temperature, e.g. in springtime or autumn. Because built-in rails cannot elongate and shrink with increasing and decreasing temperatures, seasonal differences in the temperature will produce axial thermal stresses. These are tensile stresses at lower and compressive stresses at higher temperatures. Residual stresses in rails are introduced by different mechanisms. Primarily they stem from the manufacturing process, namely from heat treatment and roller straightening.

## 1.2. Statement of the Problem

While many parts may work well initially, they often fail in service due to fatigue failure caused by repeated cyclic loading. In practice, loads significantly below static limits can cause failure if the load is repeated sufficient times. Thus, Wheel-rail rolling contact is subjected to repeated mechanical cyclic stress, and causes in sever damages. Wheel-rail contact is subjected to a series of normal and tangential forces due to the load, Wheel-Rail profile and tractive effort. Most of wheel-rail contact failures are caused by rolling contact fatigue. Thus, wheel-rail contact needs to have an excellent fatigue life. Characterizing the capability of a material to survive the many cycles a component may experience during its life time is the aim of fatigue analysis. Thus, intends to predict the fatigue life at the wheel-rail rolling contact using finite element method (FEM) ANSYS software. Prediction, identification and properly designed system of wheel-rail profiles that controls stress and wear provides for durable, stable, and optimized wheel-rail performance stress will be suggested.

## 1.3. Objective of the Research

### 1.3.1. General Objective

To analyze Effect of change of Rail Profile on Rolling contact fatigue stress using analytic and finite element method.

### 1.3.2. Specific Objective

- ✓ Modeling wheel and rail profiles using CATIA software
- ✓ Employing EXCEL and ANSYS software to carry out theoretical and finite element analysis considering different contact patches arising from various rail profile obtain the rolling contact fatigue stresses of each condition
    - I. To analysis fatigue damage
    - II. To predict fatigue life

## 1.4 Scope of the research

This thesis covers analysis of rolling contact fatigue at wheel-rail interface. The rolling contact fatigue failure is assumed due to the mechanical loads and Track conditions is straight with rail profile (radius of curvatures) is change (280, 290, 300, 310, 320, 330mm) are taken for this investigations. The effect of variations in the rail profile considered for The fatigue analysis based on the stress life. For the fatigue analysis 3D finite element method ANSYS software is used.

## 1.5. Significant of the study

The thesis is very valuable for fatigue resistance design and inspection planning for wheel and rail interaction.

## 1.6 Research methodology

To achieve the scope of the thesis the following methodological approaches are performed.

### 1.6.1. Data collection:

Necessaries data and specifications are gathered from AA LRT project office. And also different articles, journals, and other related documents are used to perform the thesis work.

### 1.6.2. Data analysis:

Analyses of Effect of Variation Wheel-Rail Contact Profiles on Contact Fatigue Stress have several theoretical and numerical approaches on wheel rail contact are employed to investigate the relationship between different Radius Curvature of wheel and rail with fatigue Life of Wheel-Rail Contact. These are:

- ✓ Hertzman theory of contact for the normal problem (i.e. determinations of elliptical contact patch and contact stresses).
- ✓ The Dang Van criterion based on the Wohler (S-N) curve is employed in order to quantify the fatigue Damage.
- ✓ Finite element software ANSYS 15.0 and EXCEL are employed for numerical results
- ✓ For modeling of wheel and rail CATIA V5 R16 is used

### 1.6.3. Result presentation:

For easily readable and clearly understandable for readers, the obtained results are presented in tables, graphs and plots form.

## 1.7 Thesis layout

The thesis focuses on the analysis of rolling contact fatigue at the wheel-rail contact. And it has five chapters. The first chapter is the introduction part which clearly describes the general of the study, statement of the problem, and objective, scope of the study, and research methodology, the second chapter describes related literature reviews about the thesis topic; analysis of rolling contact fatigue at the wheel-rail interface. These literature reviews are basics for the present thesis, the third chapter contains the collected data and specifications and the analysis of forces at different Rail Profile (at radius of curvatures (280, 290, 300, 310, 320, 330mm). The aim of this chapter is to obtain the input contact forces for the FEA (fatigue analysis), the fourth chapter is the main body of the thesis. It includes the material mechanical properties, geometry modeling, and finite element modeling and FEA (fatigue analysis) and the next chapter presents results and discussions. In this chapter the simulated model gives results in counter plots and the obtained results are discussed one by one in tables and graphs form and the last chapter describes briefly the conclusion, recommendations, and future works of the thesis.

# Chapter Two

## Literature Review

The study of rolling contact, or more accurately rolling-sliding contact, is said to be started in 1926 by the publication of Carter's paper [F. Carter, 1926] on the solution of the two-dimensional rolling contact problem. The three-dimensional rolling contact including sliding was touched upon by Johnson [K. Johnson, 1985] about thirty years later. His theory was approximate. Kalker continued to study the subject. He published several theories among which there is a complete theory of three-dimensional rolling contact. Using his theory, it is possible to solve the problem numerically. However, his theory is limited by the half-space assumption. Later on, others like [Wriggers, 2002] studied the problem using FEM. Using FEM, the half-space limitation is lifted and material non-linearity can be included as well. However, it raises other issues to be dealt with.

The size and shape of the contact zone where the railway wheel meets the rail can be calculated with different techniques. Traditionally, the Hertz theory of elliptical contacts has been used implying the following assumptions: the contact surfaces are smooth and can be described by second degree surfaces; the material model is linear elastic and there is no friction between the contacting surfaces; and the contacting bodies are assumed to deform as infinite half spaces. The half space assumption puts geometrical limitations on the contact, i.e., the significant dimensions of the contact area must be small compared with the relative radii of the curvature of each body. Especially in the gauge corner of the rail profile, the half plane assumption is questionable since the contact radius here can be as small as 10 mm. Due to its simple closed form solutions; the Hertz method is the most commonly used approach in vehicle dynamics simulation. However, other methods are used for simulation of wear and surface fatigue due to the overestimation of the contact stresses attributed to the no validity of the half plane assumption and nonlinear material behavior. Kalker's numerical program Contact still depends on the half space assumption, but is not restricted to elliptical contact zones. The contact surfaces are meshed into rectangular elements with constant normal and tangential stresses in each rectangular element. Telliskivi and Olofsson developed a finite element model, including plastic deformation, of the wheel – rail contact using measured wheel and rail profiles as input data. And this was illustrated in [Ulf Olofsson and Roger Lewis, 2006]

According to [Paul Boyd, 2002] the entire body of knowledge relating to contact mechanics can be traced back to the initial work done by Hertz on a simplified contact model. These initial theories were based on the theories of elasticity which were well established and were further enhanced by the development of the theories of plasticity. Kalker produced the next most significant contribution to the discipline of contact mechanics with his expansion of Hertz theories and the development of computer algorithms specifically concerned with the calculation of railway rail/wheel surface tractions which are used extensively in multi body dynamics software to provide the linkage between the railway rail and wheel.

The FEM analysis is the ultimate available solution to the contact problems which violates the underlying assumptions of Kalker's variation method. It is not bound to half-space assumption and various material properties can be considered. Moreover, more detailed friction laws than the well-known Coulomb's law can be used. However, like any numerical method, there are several numerical issues to be dealt with. [Matin Shahzamanian Sichani, 2013]

According to [Shahzamanian Sichani, 2013] FEM is a numerical method to solve partial differential equations (PDEs). It eliminates the spatial derivatives and converts the PDE into a system of algebraic equations. To do so, the bodies under investigation, considered as a continuum, are discredited into elements with certain number of nodes. The solution to the PDE using FEM is exact at the nodes; while in between the nodes it is approximated by polynomials known as shape functions. One of the fundamental issues to deal with when investigating the wheel rail contact is the rolling contact fatigue (RCF) phenomenon. It must be emphasized that (RCF) cannot be evaluated based on normal contact stress alone since the interdependence with tractions and material strength is too intimate. According to [Eric Magel, Peter Sroba,2006] Assessing wheel/rail performance with respect to contact fatigue requires consideration of all three parameters namely: Normal stress (Po) at wheel/rail contact which is a function of four main factors; wheel diameter, wheel load (including possible dynamic loading), the transverse rail profile and the transverse profile of the wheel. Rail/wheel tractions (T/N*)* which develops due to small relative slip between the rail and wheel that shears the interfacial layer in the contact zone. The level of slip (also known as creep) depends on the curving and traction demands. Rail metallurgy in laboratory studies generally recur two conclusions. First, for a given level of hardness, pearl tic steels are more

resistant to RCF than are other structures such as binate and marten site. Second, for any given type of steel structure, resistance to RCF increases with hardness. Much work has been carried out on wheel and rail failure due to fatigue, wear and the action of wheel and rail defects. Again these effects rely on the understanding of the stress fields present and constitute another direction for the application of this research. [Ekberg et al,1995] cites the need for accurate surface, subsurface and residual stresses in his "fatigue model for general rolling contact with application to wheel/rail damage" and cites the applications of FEA programs such as ABAQUS as suitable. [Magnus et al, 1993] also describes a model for cyclic ratcheting plasticity and the development and propagation of fatigue cracks using the ABAQUS code which appears to indicate that ABAQUS may be the software of choice for this work.

Several parameters influence the stress state in rails as illustrated in[Marine Vidaud,2009]: A non-exhaustive list of these parameters might be: axle load; asymmetric loadings where the strain will also be posed asymmetric on the rail head and the rail wheel contact will get irregular and discontinuous; wheel diameter including mismatched wheel diameters; track gauge; wheel transversal profile; rail transversal profile and profile irregularities; cant excess/deficiency where wheel sets will tend to shift and to heavily offset to the inner or outer rail respectively; welds where at too soft/flexible welds a dip will be produced or, in case too hard high spots will be produced this will both leading to geometry irregularities; hunting of wheel set in tangent tracks; string lining forces on grades tie plate cut in and poor fastening; Skewed trucks.

In the contact zone between railway wheel and rail the surfaces and bulk material must be strong enough to resist the normal (vertical) forces introduced by heavy loads and the dynamic response induced by track and wheel irregularities. The tangential forces in the contact zone must be low enough to allow moving heavy loads with little resistance, at the same time the tangential loads must be high enough to provide traction, braking, and steering of the trains. [Ulf Olofsson and The first step in wheel/rail profile evaluation procedure is the realization of a multi body model of the complete railway vehicle and track combination. This is performed to evaluate contact specific parameters, such as wheel/rail forces, relative positions, and creepages. This was discussed in detail on [Iwnicki S. ed., 2006]

An important characteristic of contact between wheel and rail is the rolling radius of the wheel at the contact point. Consequently, the difference between the rolling radius of the right and the left wheel (rolling radius difference or RRD) as a function of the lateral displacement of a wheel set is one of the main characteristics of wheel/rail contact that defines the behavior of a wheel set on a track. Modeling of the wheel rail contact both analytical and finite element simulation software's using rolling radius difference as a function of wheel and rail profiles were shown on. [Ivan Y.

In computational modeling of railway vehicle, modification of the rolling radius difference (RRD) function can change dynamic behavior of the wheel set helping to achieve the required performance. This modified RRD function virtually corresponds to a new combination of wheel/rail profiles. For a given rail profile, one may solve the inverse problem in order to find a wheel profile to match the modified RRD function. The inverse problem can be solved using an optimization method. This idea was used as a strategic concept in the creation of the procedure for wheel profile design on [Ivan Y. Shevtsov, 2008].

For analyzing the dynamic behavior of railway vehicles running on arbitrary tracks under arbitrary maneuvers, usually the vehicle (and maybe the necessary environment) is abstracted basically as a multi body system. According to [Gunter Schupp , 2007], A multi body system consists of rigid or elastic bodies, interconnected via mass less force elements and joints. Due to the relative motion of the system's bodies, force elements generate applied forces and torques. Typical examples are springs, dampers and actuators combined to primary and secondary suspensions of railway vehicles. Contrarily, joints give rise to constraint forces by constraining the relative motion of the system's bodies. The scope of applications starts with simple single axis rotational joints and ends with highly complicated and specific ones like the so–called wheel–rail joints' guiding bodies along arbitrary tracks. Usually, the user can rely on extensive libraries of connecting elements while setting up the simulation model.

Carter described a simple 2D contact surface, but he was the first to give a rather adequate expression of the force relative to the creep age in the longitudinal direction. His method of describing the stresses in the adhesive zone was used until the 1960s. Fromm made similar observations. Rocard described the linear relationship between the yaw angle and the guiding

force, for rubber tires and for railway wheels, in the lateral direction. He was particularly interested in the equivalent of the bogie hunting for cars: the shimmy phenomenon.

In the 1960s, more experimental data were available; the definitive expressions were established mainly by Johnson and Kalker, who gave an expression of the creep age stiffness introducing variable coefficients depending on the b/ ratio of the contact ellipse.

Subsurface initiated rolling contact fatigue is assessed using the FIERCE model [Ekberg et al., 2002]. The fast algorithms in FIERCE allow for fatigue evaluation in each time increment. This facilitates a statistical evaluation of the fatigue impact, which is of major importance in the study of RCF of railway wheels: Since the wheels are travelling along a track with varying characteristics, they will be subjected to a broad spectrum of fatigue loading. From a fatigue point of view, mainly extreme loads are of importance since, first, fatigue initiation is related to magnitudes of fatigue impact exceeding the (equivalent) fatigue limit and, second, above the fatigue limit life is decreasing exponentially with the increase in fatigue loading.

If we look at RCF initiation deeper into the wheel rim, interfacial wheel-rail friction and the size and shape of the contact patch will have less influence. Instead, the magnitude of the total contact load and the occurrence of material defects will be the main influential factors [Kabo, 2002; Kabo and Ekberg, 2005].

[Michael Gmariam, 2013] has also studied the effect of change of contact ratios on contact fatigue stresses on spur gears. In his study he considered different cases of six contact ratios gearing between 1.6 and 2. For the different contact ratios considered different stress conditions are determined. ANSYS and CATIA finite element software's are used for finite element result

# Chapter Three

## Analysis Method and Condition

### 3.1 Wheel and Rail Material Properties

Around the world, there are various manufacturers of wheel and rail materials. Wheel and rail materials are quite similar in composition, differing slightly in the amounts of carbon, silica, and manganese in the steels used. It is widely known in tribology that pairs of similar metals can exhibit high adhesion and should generally be avoided in applications where they come into contact with each other [27], so changing one of these materials might reduce wheel and rail wear.

However, there are other damage mechanisms to consider except wear when discussing the material properties, for example rolling contact fatigue and corrugation. Wear resistance is considered one of the most important characteristics of a rail steel. Pearlite steel is the most widely used such steel, as the pearl tic microstructure resists wear and rolling contact fatigue [28]. Another important feature of wheel and rail materials is inclusions, which may cause cracking and high wear rates. In other types of materials, such as the nodular cast iron, carbon nodules are naturally embedded in the material. Railway wheels made of au tempered ductile iron (ADI) containing graphite nodules were studied by Kuna et al. [29] and Madder [30], who found that this material combines the advantages of high wear resistance and high fatigue strength with the wear-reducing side effect of the graphite inclusions,

The main disadvantage of au tempered ductile iron is that its fracture toughness is lower than that of the steels regularly used in the wheel–rail contact. In some contexts, ductile iron is also called nodular cast iron. Madder [35] reports that ADI has been used by the Finnish National Rail System for railway wheels. Its use reduced life-cycle costs, but also resulted in some wheel tread failures [31]. Using measurements made in the field and the experimental results of pin-on-disc and twin-disc testing, Lewis and Olausson [28] found that the introduction of more modern rail materials has reduced the wear rate by up to an order of magnitude over the last 20 years. This finding highlights the importance of high-performance wheel and rail steels. Coatings have been demonstrated to have a positive effect on product longevity under severe conditions. Rings conducted theoretical, laboratory, and field studies of surface coatings on rails in highly loaded

wheel/rail contacts and found reductions in rolling contact fatigue (RCF) damage and wear. Concerning their chemical compositions rails have great varieties of carbon, manganese, chromium and silicon contents depending on their requirements. Since the rails have to withstand the impact load, friction and stress of freights, they should have sufficient strength, hardness, toughness and good welding performance. However, a large increase in rail mechanical strength may result brittle failure and as a result a further increase is not desirable. Similarly, the same material property is selected for wheel –rail materials. For Addis Ababa light rail transit (AA LRT), the rail standard used is China National Railways standard of 50 kg/m.

## 3.2. Material Selection

The railway tracks are mostly steel material in accordance to the EN 13674-1:2011 (E). Steel is the most common and widely used metallic material in modern society. It can be produced with tensile strengths exceeding 5 GPa. Steel contains 50% iron and one or more alloying element. These elements generally include carbon, manganese, silicon, chromium, phosphorus, Sulphur etc. Each chemical element has a specific role in the steel making process or in achieving particular properties or characteristics. E.g. Strength, hardness and quality. In this study, the material of rail used in AA-LRT is U71Mn, which is equivalent to R260Mn and its mechanical property and the chemical composition are discussed on the table 4.1 and 4.2 respectively. Rail material rail property in accordance to EN 13674-1:2011

**Table 3.1 Mechanical property of rail material**

| Material Property | Value |
|---|---|
| Poison Ration | 0.3 |
| Ultimate tensile strength $\delta_{ut}$ for (wheel and rail) | 900Mpa |
| Tensile Yield strength $\delta_y$ for(wheel and rail) | 640Mpa |
| Young modulus | 207Gpa |
| density | 7800KG/$m^3$ |

**Table 3.2 Chemical composition of rail**

| item | 1 | 2 | 3 | 4 | 5 | 6 | 7 |
|---|---|---|---|---|---|---|---|
| Chemical element | c | si | cr | Mn | p | s | Al |
| composition | 0.65 -0.76 | 0.15 -0.58 | -- | 0.70 -1.20 | <0.04 | <0.025 | <0.010 |

**Table 3.3 Mechanical property of wheel material**

| Material Property | Value |
|---|---|
| Poison Ration | 0.3 |
| Ultimate tensile strength $\delta_{ut}$ for (wheel and rail) | 900Mpa |
| Tensile Yield strength $\delta_y$ for(wheel and rail) | >580Mpa |
| Young modulus | 207Gpa |
| density | 7800KG/$m^3$ |

**Table 3.4 Chemical composition of wheel**

| item | 1 | 2 | 3 | 4 | 5 | 6 | 7 | 8 | 9 | 10 |
|---|---|---|---|---|---|---|---|---|---|---|
| Chemical element | c | si | cr | Mn | p | s | cu | Mo | Ni | V |
| composition | 0.6 | 0.4 | 0.03 | 0.8 | 0.04 | 0.04 | 0.3 | 0.08 | 0.30 | 0.50 |

## 3.3 Hertzman Contact theory

Contact when a wheel and a rail are brought into contact under the action of the static wheel load, the contact area and the pressure distribution is usually determined using the Hertz theory. In Hertz contact theory, no plastic deformation in the contact patch is assumed, and the radii of the curvature of wheel and rail profiles in the contact patch are assumed to be constant. According to Hertz theory, the normal pressure is distributed as an ellipsoid over elliptic contact area. The distribution of contact pressure in can be expirees Dimensions of Wheel and Rail.

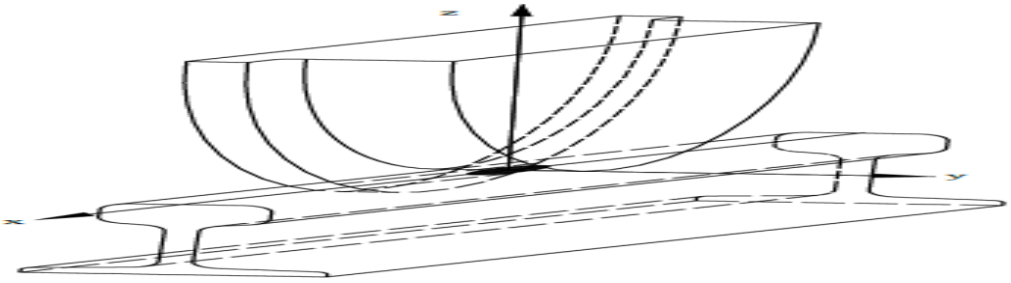

**Figure 3.1: wheel rail contact**

Where, **Fz** is the applied normal load at the contact, **a** and **b** are semi axes of the contact ellipse, the magnitudes of *a* and *b* depend on the normal load, wheel and rail profiles and materials. X and Y are the required coordinates to specify the point of contacts on the rail surface based on the lateral rail surface parameter. The contact ellipse semi-axes **a** and **b** is determined as follows: According to Hertz theory, the normal pressure is distributed as an ellipsoid over the elliptic contact area. The ellipsoidal normal contact pressure distribution p(x, y)

## 3.4 Mathematical model for Wheel–Rail Contact

First, according to Yan [13], if two elastic nonconforming bodies are pressed together then the contact area assumes elliptical shape with a semi major axis '**a**' and semi minor axis '**b'** The distribution of the contact pressure in this elliptical area. In the railway field, the maximum contact pressure is frequently. This frequently contact pressure is over the elastic limit of most steels, but the compression state is more complex than a simple tensile test and the elastic limit is not reached. The determination of the plasticization must be calculated with a criterion based on the stress

The pressure distribution within the contact ellipse will be given by:

$$P(x,y) = P_O\sqrt{1-\frac{x^2}{a^2}+\frac{y^2}{b^2}} \quad \text{..... 3.1.1}$$

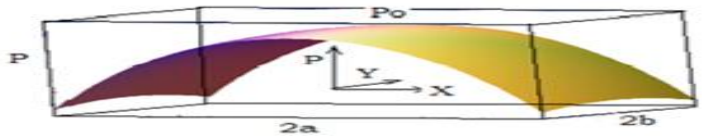


**Figure 3.2: Pressure distribution across elliptic area**

The distribution of pressure P is found by assuming the intensity of pressure over the surface of contact to be represented by the ordinates of a semi-ellipsoid constructed on the surface of contact. The maximum pressure is obtained by satisfying roots of the Eq. (3.1.1), occurs at the center of the surface of contact is given by Depend on the material properties of railway wheel and rail respectively. Where the maximum contact pressure acts at the center of the elliptical contact area is computed in

$$Po = \frac{3FN}{2\pi ab} \quad \text{.....3.1.2}$$

The semi axes of the elliptic boundary of the surface of contact '**a', 'b'** are given by

$$a = \sqrt[m3]{\frac{3\pi F(k_1+k_2)}{4(A+B)}} \quad \text{..... 3.1.3}$$

$$b = \sqrt[n3]{\frac{3\pi F(K_1+K_2)}{4(A+B)}} \quad \text{.....3.1.4}$$

The calculation of the contact areas requires knowledge of some geometric constants used in the above formulation. With respect to wheel-rail configuration, the following curvature combinations are related as:

To calculate 'a'**, 'b'** first let's find the values of $K_1$ and $K_2$ are constants that depend on the material properties of railway wheel and rail respectively.

$$K_1 = \frac{1-V_1^2}{\pi E_1} \quad \text{.....3.1.5}$$

$$K_2 = \frac{1-V_2^2}{\pi E_2} \quad \text{..... 3.1.6}$$

$$K_3 = A+B = \frac{1}{2}\left(\frac{1}{R_{11}}+\frac{1}{R_{12}''}+\frac{1}{R_{22}}+\frac{1}{R_{21}''}\right) \quad \text{.....3.1.7}$$

$$K_4 = A-B = \frac{1}{2}\sqrt{\left(\frac{1}{R_{11}}-\frac{1}{R_{12}''}\right)^2+\left(\frac{1}{R_{22}}-\frac{1}{R_{21}''}\right)^2+2\left(\frac{1}{R_{11}}-\frac{1}{R_{12}''}\right)\left(\frac{1}{R_{22}}-\frac{1}{R_{21}''}\right)(\cos(2\Psi))} \quad \text{.....3.1.8}$$

$$\text{Cos}(\theta) = \frac{B-A}{A+B} \quad \text{.....3.1.9}$$

$R_{11}$, $R_{12}$, $R_{21}$and $R_{22}$ are defined as the principal relative radii of curvature, represented pictorially in the Fig. **3.3**

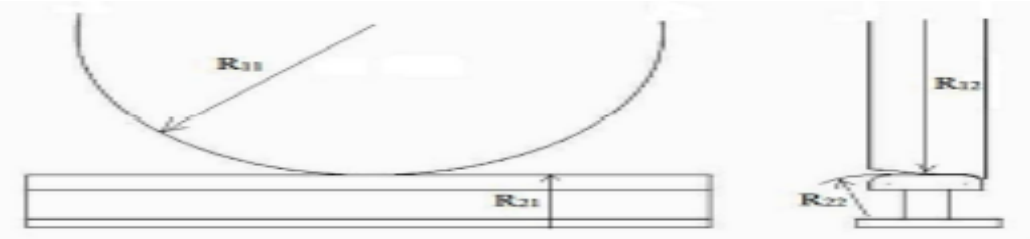


**Figure 3.3: Wheel-Rail Configuration of different principal relative radii of curvature**.

Where,

$R_{11}$: The rolling radius of curvature of the wheel.

$R_{12}$: The radius of the wheel profile, which goes to infinity for a conical wheel.

$R_{21}$: The radius of the runway which is infinity in this case.

$R_{22}$: The radius of curvature of the rail in the plane of cross section.

The principal direct stresses acting along the z, x, y axes at or below, the contact center are: For an elliptical contact, direct stresses along the principal planes at the center of contact surface are:

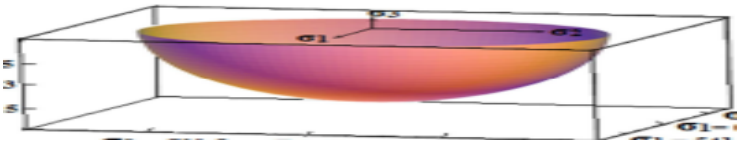

**Figure 3.4: Stress Ellipsoid**

The principal direct stresses acting along the z,x,y axes at or below ,the contact center are: δx, δy, and δz .The shear stress acting along these axes at or below the contact center is δx, δy, and δz zero. The principal shear stresses act on the planes bisecting the angle between the z,x,y planes. Their magnitude by Teresa's criterion is given by:

$\frac{\delta z-\delta x}{2}$ in the zx plane ... ... ... ... ...... ... ... ... ... ... ... ... ... ... ... ... ... ... ... ... ... ... ... ...3.2.0

$\frac{\delta x-\delta y}{2}$ in the xy plane ……..……3.2.1

$\frac{\delta y-\delta z}{2}$ in the yz plane ……..3.2.2

For an elliptical contact, direct stresses along The principal stresses at the center of the surface of contact are calculated as

$\delta_1 = 2\mu p_o + (1- 2\mu)\, p_o \frac{b}{a+b}$ ……3.2.3

$\delta_2 = 2\mu p_o + (1- 2\mu)\, p_o \frac{a}{a+b}$ ……3.3.4

$\delta_3 = p_o$ ……3.3.5

The maximum shear stress is given by,

$\tau_{max} = \frac{po}{3} = \frac{N}{2\pi ab}$ ……3.3.6

As the principal shear stress in the plane of deformation $\tau_1 = po(\frac{F}{N})$ =K, then material throughout the width of the contact surface will begin to yield where F is the tangential creep force.

## 3.5 Teresa's and Von Mises criteria of plastic deformation

With complex stress systems, the state of stress can always be described in terms of the three principal stresses δ1, δ2, and δ3. Yield criteria then define conditions where plastic behavior is initiated for any combination of these stresses; only sudden initiation of yield is considered.

Two criteria are commonly used: Teresa's and Von Mises

The Teresa criterion states that "plastic behavior occurs when the maximum shear stresses reach a critical value. If the three principal stresses are δ1, δ2, and δ3

The maximum shear stress = $\frac{\delta 1 - \delta 2}{2}$ ……3.3.7

For uni-axial tension (in one direction) δ2= δ3=0 and δ1=Y, the yield stress in simple tension, then the maximum shear stress becomes $\frac{\delta 1}{2}$(i.e. $\tau_1 = \frac{\delta 1}{2} = \frac{Y}{2}$) for pure shear where k is the yield stress in simple shear δ2=0 and δ1= - δ3= k, then the maximum shear stress becomes δ1 (i.e. $\tau_1 = \delta 1 = k$) Thus the Teresa criterion can be generalized as:

$(\delta 1 - \delta 2)(\delta 1 - \delta 3)(\delta 2 - \delta 3) = 2k = Y$ ……3.3.8

Von Misses criterion takes into account the fact that metals cannot be compressed in all directions and therefore the hydrostatic component $\delta h = (\frac{\delta 1 + \delta 2 + \delta 3}{3})$ must be considered. Thus the effective

principal stresses are: (δ1- δh) (δ2- δh) and (δ3- δh). The criterion states that deformation occurs when this reaches a critical value that is:

$(\delta 1- \delta h)^2 + (\delta 2- \delta h)^2 + (\delta 3- \delta h)^2 = \frac{(\delta 1- \delta h)^2 + (\delta 2- \delta h)^2 + (\delta 3- \delta h)^2}{3}$ = constant

Again considering the case of uni axial tension, where δ2 = δ3=0 and δ1=Y

The constant becomes $\frac{2\,(Y)^2}{3}$.

From the case of pure shear, (δ2 =0 and δ1= - δ3= k) the constant becomes $2(k)^2$ Therefore for Von Mises case k=0.58Y

$(\delta 1- \delta 2)^2 + (\delta 1- \delta 3)^2 + (\delta 3- \delta 1)^2 = 2(Y)^2 = 6k^2$……...3.3.9

This differs slightly from Teresa. Although refined experiments with ductile metals tend to support Von Mises, as the difference is small and most metals are not fully isotropic, Teresa is usually used for algebraic simplicity.

## 3.6 prediction of wheel fatigue

There are a multitude of different numerical models to analyze wheel fatigue reported in the literature. Here, the presentation will focus on general stress fatigue in the wheel rim. Only some selected models are presented which have the benefit of being described in analytical form.

## 3.7 Subsurface-initiated rolling contact fatigue

To facilitate the prediction of subsurface-initiated RCF, we will distinguish between the cases of shallow initiation (say, from some 4 mm to some 10 mm below the wheel tread) and deep initiation (say, at some 10-25 mm below the tread).

For the shallow cracks we presume fatigue initiation to be related to the magnitude of the shear stress. Assuming Hertzman contact conditions, the maximum shear stress will occur some millimeters below the tread surface and have an approximate magnitude of

$$\tau_{max} = \frac{po}{3} = \frac{N}{2\pi ab}$$……..3.4.0

Here, po is the peak normal contact pressure, N the total normal contact load 'a', 'b' and the semi-axes of the Hertzman contact patch. Since the state of stress in the wheel rim is multi axial, an equivalent stress criterion will be employed to quantify the fatigue impact. Here, we use a multi axial fatigue criterion (Dang Van et al., 1989), which can be expressed as:

$\delta_{EQ} = \tau a + \alpha DV \delta h$ ..... 3.4.1

αDV is a material parameter that may be evaluated as:

$\alpha DV = \frac{3\tau e}{\delta e} - \frac{3}{2}$ ..... 3.4.2

Where τe the fatigue limit in alternating is shear, and $\delta e$ is the fatigue limit in rotating bending

$\delta h = \frac{\delta x + \delta y + \delta z}{3}$ ..... 3.4.3

Where δh is the hydrostatic stress (positive in tension).

For wheel-rail contact conditions there is a pulsating shear stress evolution on the shear plane experiencing the highest 'amplitude'. The shear stress 'amplitude' τa is for this case half of the maximum shear stress $(\tau a)_{max} = \frac{\tau \max}{2} = \frac{N}{4\pi ab}$ If additional frictional loading of moderate magnitude is applied, the maximum shear stress may be estimated at:

$\tau_{max} = \frac{N}{2\pi ab} (1+f^2)$ ..... 3.4.4

Here $f = \frac{\sqrt{Fx^2 + Fy^2}}{N}$ where Fx and Fy are tangential forces.

Combining Esq. (3.3.9) and (3.4.0), the equivalent stress can be expressed as:

$\delta_{EQ} = \frac{N}{4\pi ab} (1+f^2) + \alpha DV \ \delta h \ res$ ..... 3.4.5

Where δh res is the hydrostatic part of the residual stress.

Fatigue is predicted to occur if $\delta_{EQ} > \tau e$ where τe is the fatigue limit in shear, which is roughly $\frac{\delta u}{3}$ where δu is the tensile fracture stress of the material. As seen above, the size of contact patch *(π*ab*)* will influence the magnitude of the fatigue impact

($\delta_{EQ}$). In addition, the shape of the contact patch will have an influence. In wheel-rail contact, the patch is normally elongated in the rolling direction. If we look at RCF initiation deeper into the

wheel rim, interfacial wheel-rail friction and the size and shape of the contact patch will have less influence. Instead, the magnitude of the total contact load and the occurrence of material defects will be the main influential factors which will not be presented in this paper.

### 3.8 fatigue damage per cycle, D

The other parameter used to quantify the fatigue impact is the concept of fatigue damage. For one stress cycle the fatigue damage can be defined as D=1/Nf, where Nf is the fatigue life in terms of stress cycle for the current stress amplitude. Fatigue failure is then assumed to occur at a material point when the total accumulated amount of damage D attains the value 1(unity). When the equivalent stress in a material point exceeds a certain value, it is postulated that fatigue damage will occur. The amount of fatigue damage that will be induced is quantified using an approach setting out from the Wohler curve or (S-N) curve in short. It assumed that the equivalent fatigue limit, σ , corresponds to 106 stress cycles and that an equivalent stress level corresponding to the ultimate (equivalent strength),δu corresponding to 101 stress cycles .the fatigue damage per cycle corresponding to an equivalent stress level $\delta_{EQ}$ can be expressed as :

$$D = 10^{\frac{5(\delta e-\delta EQ)}{\delta e-Su}-6} \quad \text{3.4.6}$$

$$N_f = \frac{1}{D} \quad \text{3.4.7}$$

Naturally more accurate results cannot be estimated using this approach since the Dang Van equivalent stress only reflects the fatigue behavior of the material for load magnitude close to the fatigue limit. The approach will however reflect the exponential growth of the fatigue damage with stress magnitude which in turn is also a function of other parameters such as the geometrical size of load contact patch. Researches were carried out to understand and model wheel/rail wear behavior. Empirical studies, both on a full-scale laboratory test rig and in the field have shown that the wear of wheels and rails depends on the rate of dissipation of energy within the contact patch

# Chapter Four

## Analysis Results and Discussion

### 4.1 Analysis and Acceptable Standards

Rails as an important part of the railway infrastructure have exact level of quality. In Europe, the quality of rails is prescribed by international standards, the European Union of Railways UIC 860 and EN13674. [Bratislava Sladojevic, 2010]. For the analysis, all standard data for the rail profile are gathered from China, Japanese and Russian in accordance to the (GB50KG, GB 43KG), (JIS 37KG JIS 40KG), (GOST P 60KG GOST P 65KG) respectively.

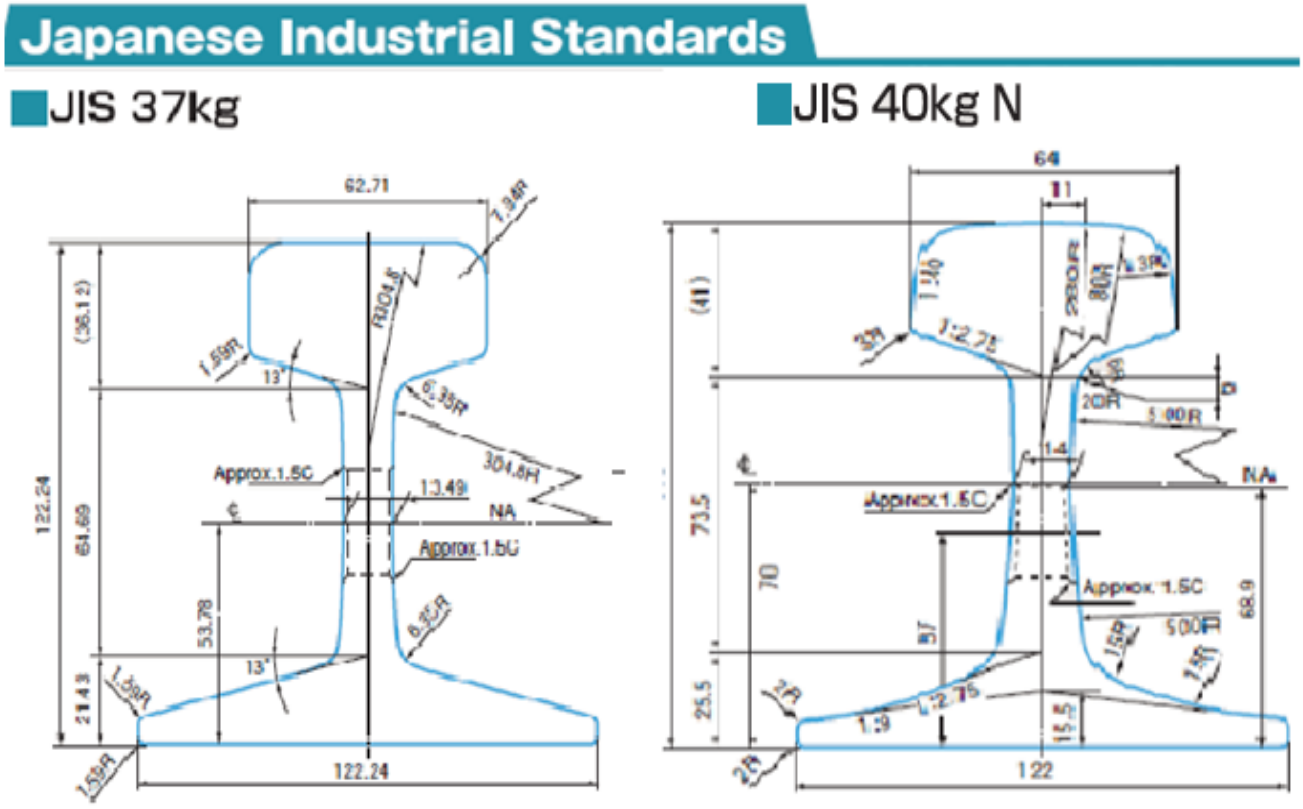


**(A) JIS 37KG 304.8R** **(B) JIS 40KG 280R**

**Figure 1.1**: Typical Japanese standard rails

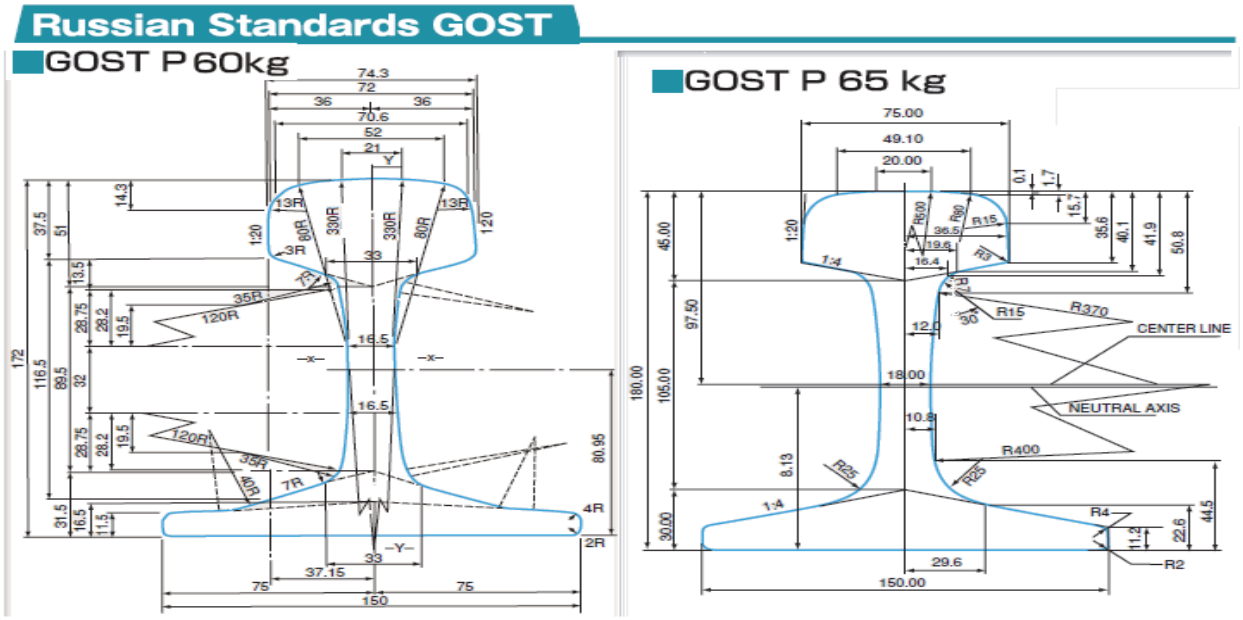


**(A) GOST P 60KG R330** **( B ) GOST P 65KG R500**

**Figure 1.5**: Typical Russian standard rails

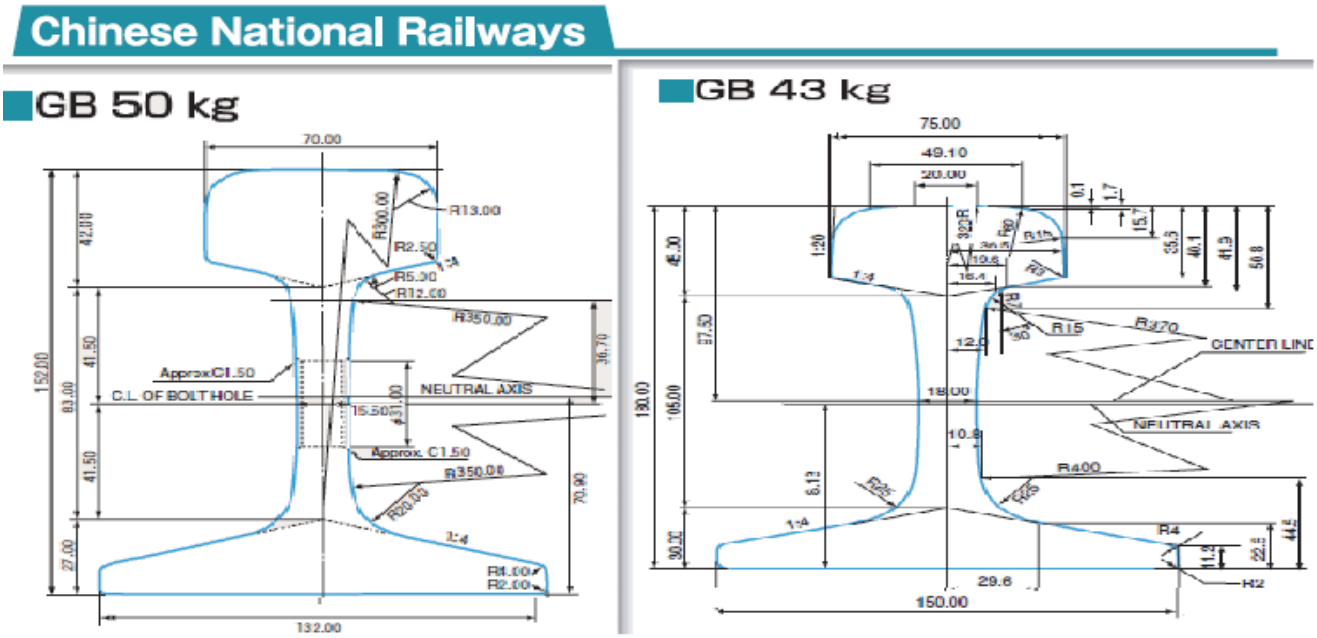


**(A) GB50KG R300** **(B) GB 43KG R320**

**Figure 1.4**: Typical Chinese standard rails

## 4.2 Theoretical results

For the analysis, the Addis Ababa LRT rail profile is using in china standard and A comparison with other rail profile standards of Japanese, and Russian Correspondingly, variations in the results in terms of stresses, contact area, and fatigue life with changes in radiuses of rail profile are obtained. The Results obtained are expected to help understand how rolling contact fatigue vary with different radiuses of rail profile. The wheel is used as per international union of railway (UIC S100) standard.

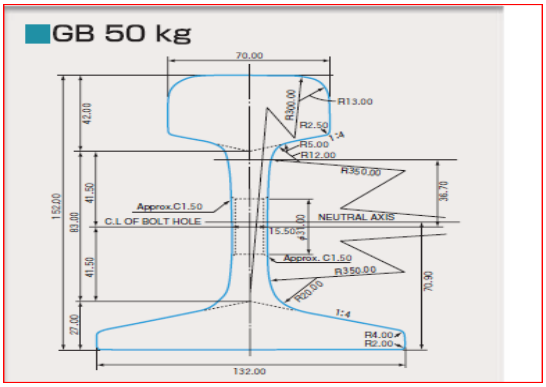


**Figure 4.5**: Rail profile in Chinese standard

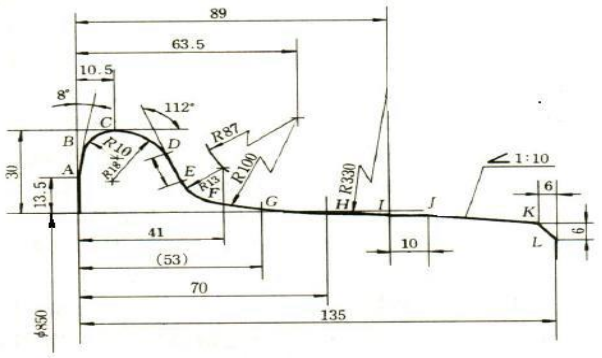


**Figure 4.6**: common wheel profile for UIC standard

### 4.2.1. Main Dimensions of Wheel and Rail

- ✓ The principal rolling radii of the wheel: $R1w$= 330 mm
- ✓ The principal transverse radii of the wheel: $R2w$= ∞
- ✓ The principal rolling radii of the rail: $R1r$= ∞
- ✓ The principal transverse radii of the rail: $R2r$ = 300 mm

(Source: Ethiopian Railway Corporation, Technical Specifications of Vehicles July 2013.)

Rail Profile as per Chinese railway standard has been chosen to analyze the Effect of change of Rail Profile on Rolling Contact Fatigue at Wheel-Rail Interface. The variations in the Rail Profile considered are Rail profile radius from 280 to 330 mm

### 4.2.3. Determination of wheel-rail contact ellipse dimensions

Depending on the size and orientation of the contact ellipse the positions of the contact point may be shifted in different directions based on the magnitude of x or y. However, based on the above general Hertz contact formula and assumptions, the stress due to wheel/rail contact decreases and becomes zero if it goes far away from the centerline of the rail head. Similarly, the wheel/rail contact stress is inversely proportional to the major and minor axis of the contact ellipse. To calculate a and b, first let's find the values of $K1$, $K2$, $A+B$ and $A-B$. $K1$ and $K2$ are constants that depend on the material properties of railway wheel and rail respectively. Where

$$K1 = \frac{1-V_1^2}{\pi E_1}.$$

$$K_2 = \frac{1-V_2^2}{\pi E_2}$$

Where $v1$ and $E1$ are Poisson's ratio and young's modulus of the railway wheel material and $v2$, and $E2$ are Poisson's ratio and young's modulus of railway rail material.

$$K_1 = \frac{1\text{-}0.3^2}{\pi\times 210\times 109 N/m2} = 1.4\times 10-12\frac{m^2}{N}$$

$$K_2 = \frac{1\text{-}0.3^2}{\pi\times 210\times 109 N/m2} = 1.4\times 10-12\frac{m^2}{N}$$

$A+B$ is a constant and depends on the geometric properties of the two bodies and is defined as follows,

$$A+B = \frac{1}{2}\left(\frac{1}{R_{11}}+\frac{1}{R_{12}^{\text{“}}}+\frac{1}{R_{22}}+\frac{1}{R_{21}^{\text{“}}}\right)$$

$R_{11}$, $R_{12}$, $R_{21}$and $R_{22}$ are defined as the principal relative radii of curvature wheel and the rail respectively,

$$A+B = \frac{1}{2}\left(\frac{1}{300}+\frac{1}{\infty}+\frac{1}{\infty}+\frac{1}{280}\right) = 0.0032/mm$$

And

$$\text{A-B} = \frac{1}{2}\sqrt{\left(\frac{1}{R_{11}} - \frac{1}{R''_{12}}\right)^2 + \left(\frac{1}{R_{22}} - \frac{1}{R''_{21}}\right)^2 + 2\left(\frac{1}{R_{11}} - \frac{1}{R''_{12}}\right)\left(\frac{1}{R_{22}} - \frac{1}{R''_{21}}\right)\left(\cos(2\Psi)\right)}$$

$\Psi$ is the angle of the orientation difference of the principle axes of the two bodies; also called yaw rotation. For a straight segment the curvature of the rail, $\Psi = 0^o$. Therefore,

$$\mathbf{A\text{-}B} = \frac{1}{2}\sqrt{\left(\frac{1}{300} - \frac{1}{\infty}\right)^2 + \left(\frac{1}{\infty} - \frac{1}{280}\right)^2 + 2\left(\frac{1}{300} - \frac{1}{\infty}\right)\left(\frac{1}{\infty} - \frac{1}{280}\right)} = 0.1515\times10-3/mm$$

For a straight rail segment, $\theta$ is defined as:

$$\mathbf{Cos\ (\theta)} = \frac{A-B}{A+B}$$

$$\boldsymbol{\theta}\mathbf{=cos-1} = \frac{0.1515\times10-3/\text{mm}}{0.0032/\text{mm}} = 87.32^0$$

By using the Hertz coefficient table and linear interpolation method the value of m and n for the selected rail can be easily obtained.

Table4.1:( Hertz Coefficients) for different angle, θ

| $\theta$(deg) | m | n | $\theta$(deg) | m | n | $\theta$(deg) | m | N |
|---|---|---|---|---|---|---|---|---|
| 0.5 | 61.4 | 0.1018 | 10 | 6.604 | 0.3112 | 60 | 1.486 | 0.717 |
| 1 | 36.89 | 0.1314 | 20 | 3.813 | 0.4125 | 65 | 1.378 | 0.759 |
| 1.5 | 27.48 | 0.1522 | 30 | 2.731 | 0.493 | 70 | 1.284 | 0.802 |
| 2 | 22.26 | 0.1691 | 35 | 2.397 | 0.530 | 75 | 1.202 | 0.846 |
| 3 | 16.5 | 0.1964 | 40 | 2.136 | 0.567 | 80 | 1.128 | 0.893 |
| 4 | 13.31 | 0.2188 | 45 | 2.926 | 0.604 | 85 | 1.061 | 0.944 |
| 6 | 9.79 | 0.2552 | 50 | 1.754 | 0.641 | 90 | 1.0 | 1.0 |
| 8 | 7.86 | 0.285 | 55 | 1.611 | 0.678 | | | |

(Source: Investigation of surface ratcheting due to rail/wheel contact (2013).)

By interpolation method, we can calculate **m** and **n**

$\theta_1$=85,$m_1$=1.06, $n_1$= 0.94, $\theta_2$=90 $m_2$= 1.0, $n_2$= 1.0

By interpolation method, we can calculate "m" and "n "

$$m = m1 + \frac{m_2 - m_1}{\theta_2 - \theta_1}(\theta - \theta 1)$$

$$m = 1.06 + \frac{1-1.06}{90-85}(87.32 - 85) = 1.0324$$

Similarly,

$$n = n1 + \frac{n_2 - n_1}{\theta_2 - \theta_1}(\theta - \theta 1)$$

$$n = 0.94 + \frac{1-0.94}{90-85}(87.32 - 85) = 0.9676$$

### 4.2.4 Load application

All load data are used based on AA-LRT [25]. Vertically downward load is sum of 3% allowance, maximum axle load. The overall load is the sum of the total tram weight and carrying capacity of the vehicle. The overall load is classified to each axle of the vehicle then the axle load is classified to each wheel vehicle. Carrying capacity of vehicle has been calculated by take average of 60kg/ person and the total rate of passenger inside of the tramcar is 317.

**Table 4.2: Seating capacity of vehicle**

| Item NO | Number of passenger(person) | Seated | Seating | total |
|---|---|---|---|---|
| 1 | Seats | 65 | 0 | 65 |
| 2 | Seating capacity (standard 6 persons/$m^2$ ) | 65 | 189 | 254 |
| 3 | Overload capacity(standard 8 persons/$m^2$) | 65 | 252 | 317 |

**Table 4.3: Vehicle weight**

| Item | load | Car body weight | passenger weight | total weight |
|---|---|---|---|---|
| 1 | Empty vehicle (ton) | 44 | 0 | 44 |
| 2 | Seating capacity (ton) | 44 | 15.24 | 59.24 |
| 3 | Overload capacity(ton) | 44 | 19.02 | 63.02 |
| 4 | Axle load | <11 (1+3%)ton | | |
| 5 | Axle number | 6 | | |

**Table 4.4: Operating speed of** Car

| Item NO | parameter | speed |
|---|---|---|
| 1 | Maximum operation speed | 70km/h |
| 2 | Average travelling speed | >20 km/h |

### 4.2.4.1 The total vertical load is calculated as follows:

- ✓ Tram car weight = 44 ton = 44000 kg

  **F**= $ma = mg$

  **F** = 44000kg∗9.81m/s$^2$

  **F** = 431640N = 431.64kN

- ✓ The load applies on each axle = $\frac{\text{Tram car weight}}{\text{Axle number}} = \frac{44\ ton}{6}$. = 7.333 ton = 7333kg = **71940N**
- ✓ The load applies on each wheel = $\frac{\text{Tram car weight}}{\text{Wheel number}} = .\frac{44\ ton}{12}$.= 3.667ton = 36667kg =**35970N**
- ✓ Carrying Capacity = 60kg/person *317 person = 19020N $= \frac{19020N}{12}$ =1585Kg= **15548.85N**
- ✓ Max Axle Load on each wheel =car weight on each wheel + Carry Capacity on each wheel
- ✓ Maximum Axle Load on each wheel = 35970N +15548.85N = **51518.85N**
- ✓ Total vertical load on each wheel = max Axle load on each wheel+3% max Axle load

  =51518.85N*1.03=**53064.4N**

Note: The maximum axle load is taken to perform the analysis. The maximum parameter is used to perform the analysis. In order to attain the accurate analysis for any application, the support and the load must be defined.

Now, the values of "**a**" and "**b**" are:

$$a = \sqrt[m3]{\frac{3\pi F(k_1+k_2)}{4(A+B)}}$$

$$a = 1.0324 \sqrt[3]{\frac{3\pi * 53064.4N * (1.4\times10-12+1.4\times10-12)}{4(0.0032)}} = \mathbf{8.3822mm}$$

$$b = \sqrt[n3]{\frac{3\pi F(K_1+K_2)}{4(A+B)}}$$

$$b = 0.9676 \sqrt[3]{\frac{3\pi * 53064.4N * (1.4\times10-12+1.4\times10-12)}{4(0.0032)}} = \mathbf{4.7776mm}$$

By using the values of a, b and the normal force, the maximum Hertz contact stress will be:

$$Po = \frac{3FN}{2\pi ab}.$$

$$Po = \frac{3 * 53064.4N}{2 * \pi * 8.3822mm * 4.7776mm}. = \mathbf{632.22Mpa}$$

### 4.2.5 Determination of principal stresses in wheel-rail contact zone.

The principal stresses at center of the surface of contact are calculated as

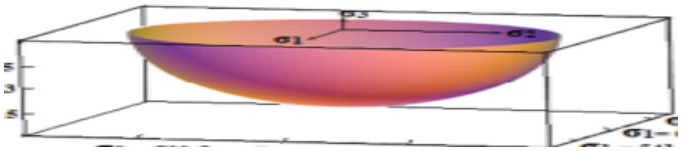

$\delta_1 = 2\mu p_o + (1- 2\mu)\, p_o \frac{b}{a+b}$

$\delta_1 = 2*0.3*649.5\text{Mpa}+(1-2*0.3)*632.22\text{Mpa} * \frac{4.7776\text{mm}}{8.3822\text{mm}+ 4.7776\text{mm}} = \mathbf{471.2Mpa}$

$\delta_2 = 2\mu p_o + (1- 2\mu)\, p_o \frac{a}{a+b}$

$\delta_2 = 2*0.3*649.5\text{Mpa}+(1-2*0.3)*632.22\text{Mpa} * \frac{8.3822\text{mm}}{8.3822\text{mm}+4.7776\text{mm}} = \mathbf{540.4Mpa}$

$\delta_3 = p_o = \mathbf{632.2Mpa}$

### 4.2.6 Determination of the equivalent stresses

Equivalent stresses at center of surface contact

$\delta eq = \frac{5}{2}\sqrt{[(\delta_1 - \delta_2)^2 + (\delta_2 - \delta_3)^2 + (\delta_3 - \delta_1)^2]}$

$\delta eq = \frac{5}{2}\sqrt{[(471.14 - 540.41)^2 + (540.41 - 632.22)^2 + (632.22 - 471.14)^2]} = \mathbf{494.82MPa}$

Accordingly, the variation in equivalent stress, fatigue damage per cycle, and expected stress fatigue life are determined using equations (3.4.5), (3.4.6), (3.4.7) respectively. The details of this calculations are summarized in table **4.5.**

Depending on the Rail profile effect on contact ellipse dimensions, size of contact patch, maximum contact pressure, principal stress, equivalent stress, fatigue damage per cycle, and expected fatigue life in the contact zone can be easily studied.

We can notice from table **4.5:** dimensions 'a' and 'b' Elliptical, contact area (πab), fatigue life Nf, increase when Rail Profile is increased. On the other hand, maximum contact pressure, principal stress, equivalent stress, fatigue damage will decrease when Rail Profile is increased.

**Table 4.5. Rail Profile influence on Wheel-Rail Contact**

| radius curvature of rail (mm) | Elliptical contact | | contact area (πab $mm^2$ | Po (MPa | $\delta_{1(X)}$ MPa | $\delta_{2(y)}$ MPa | $\delta_{3(Z)}$ MPa | δe (MPa | Fatigue damage per cycle (*10-4) | Expected fatigue life Nf, (*10+4) |
|---|---|---|---|---|---|---|---|---|---|---|
| | a major axis m | b minor axis(m | | | | | | | | |
| 280 | 8.3822 | 4.2376 | 125.811 | 632.2 | 471.2 | 540.4 | 632.2 | 498.8 | 0.266 | 5.3763 |
| 290 | 8.3841 | 4.4352 | 126.511 | 629.2 | 469.7 | 539.2 | 629.2 | 491.4 | 0.226 | 5.6818 |
| 300 | 8.3858 | 4.6113 | 127.244 | 626.3 | 468.5 | 537.3 | 624.3 | 484.1 | 0.184 | 6.0241 |
| 310 | 8.3872 | 4.7558 | 127.999 | 623.6 | 467.2 | 534.9 | 621.7 | 476.2 | 0.141 | 6.2893 |
| 320 | 8.3885 | 4.8789 | 128.711 | 620.6 | 466.3 | 532.6 | 619.9 | 467.5 | 0.103 | 6.5835 |
| 330 | 8.3899 | 4.9807 | 129.431 | 617.8 | 465.5 | 530.2 | 617.8 | 458.4 | 0.061 | 6.8114 |

## 4.2 Discussion on Results

Depending on the Rail profile effect on the contact ellipse dimensions, size of the contact patch, the maximum contact pressure, principal stress, equivalent stress, fatigue damage per cycle, and expected fatigue life in the contact zone can be easily studied. **Table 4.5** show the rail profile will be changed, some of the contact properties are increase and decrease

We can notice from table **4.5**: that the Effect of variation in the radius of curvature of rail profile on contact parameters. Increase in contact, length (major axis), width (Mainer axis), and Size of contact patch area is observed with the increase of radius of curvature of the rail profile. (See figure (4.1) (4.2) (4.3) and Contact pressure, equivalent contact stress shows reduction with increase in radius curvature of the rail profile (figure (4. 4) and (4.5).

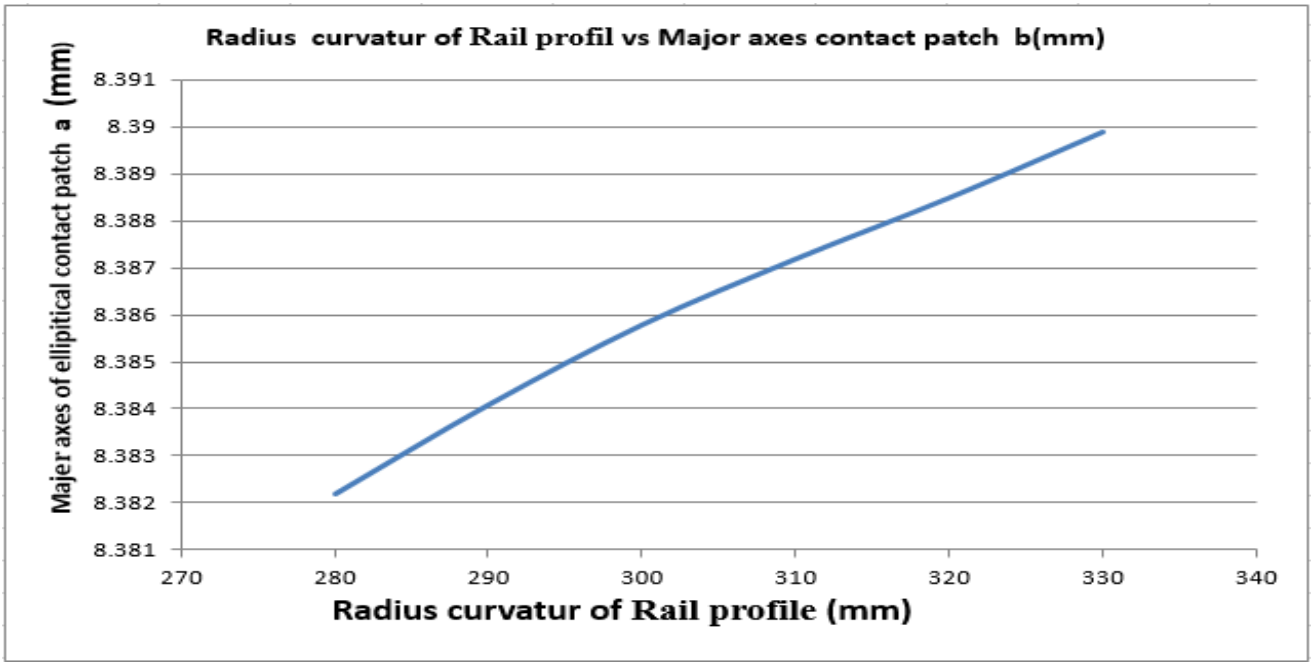


**Fig.4.1**: Shows the Increase in contact, length (major axis) with the increase of radius of curvature of the rail profile

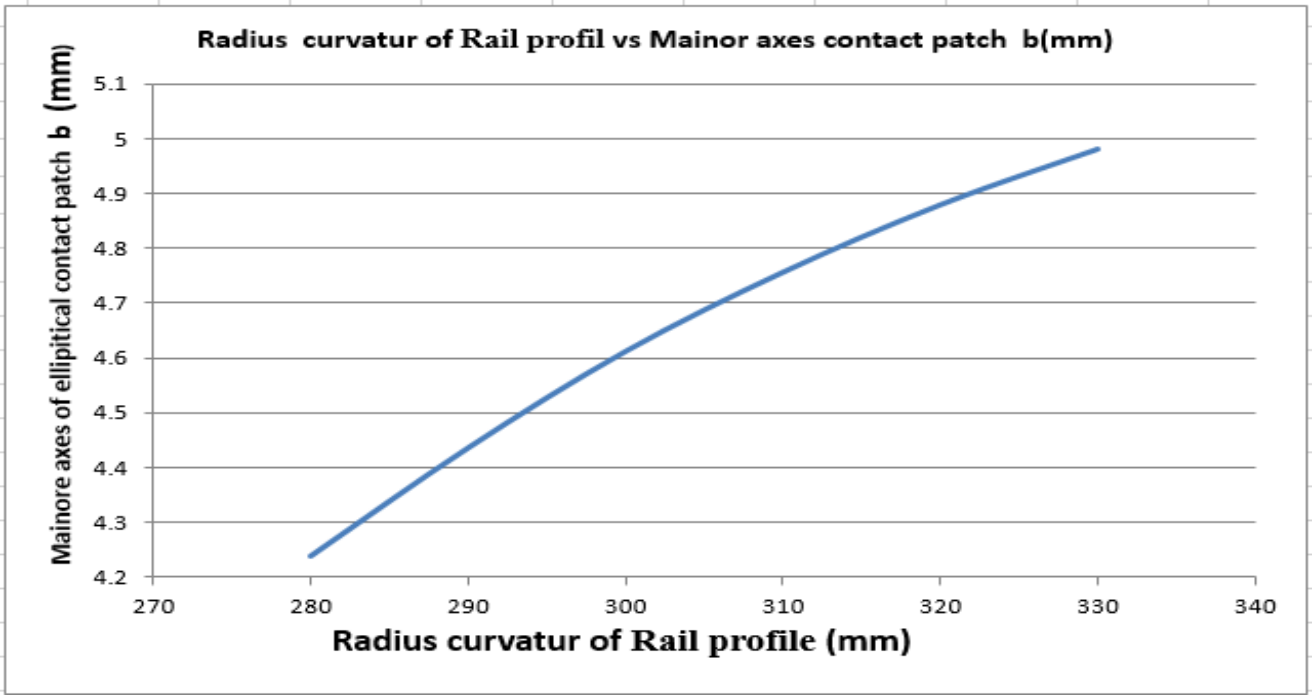


**Fig.4.2** Shows the Increase in contact, width (Mainer axis) with the increase of radius of curvature of the rail profile

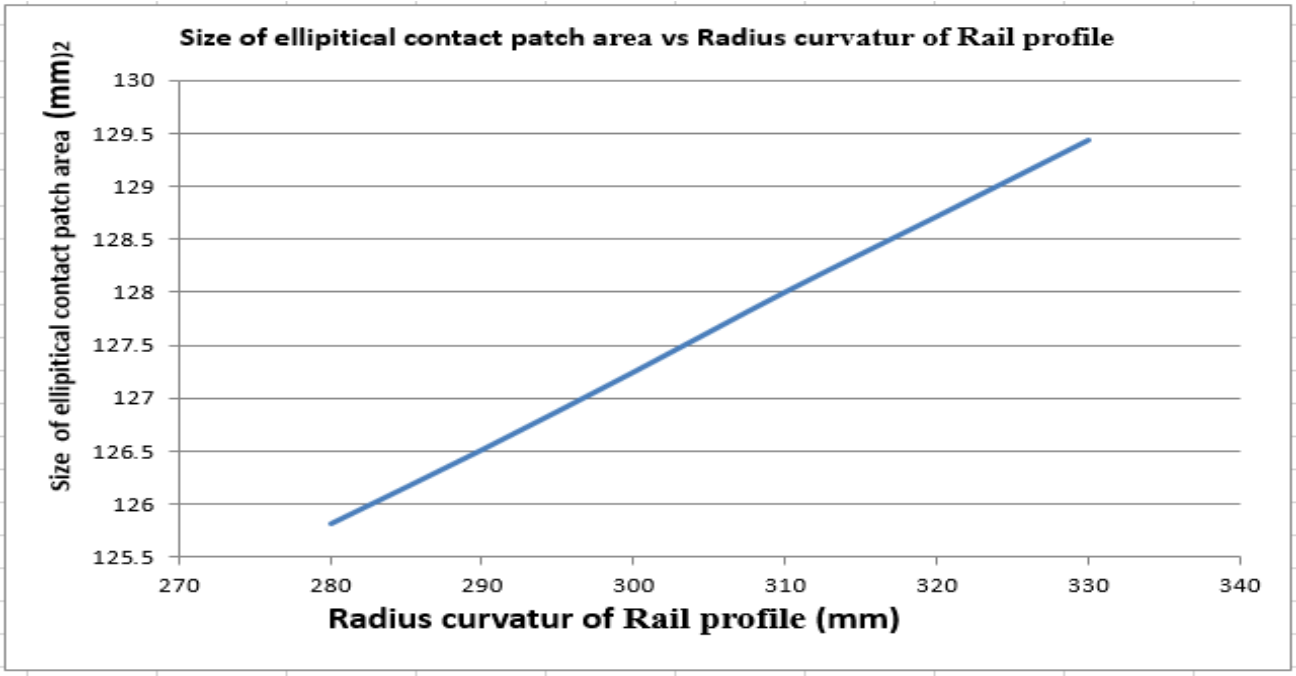


**Fig.4.3** Shows the Increase of contact patch area with the increase of radius of curvature of the rail profile

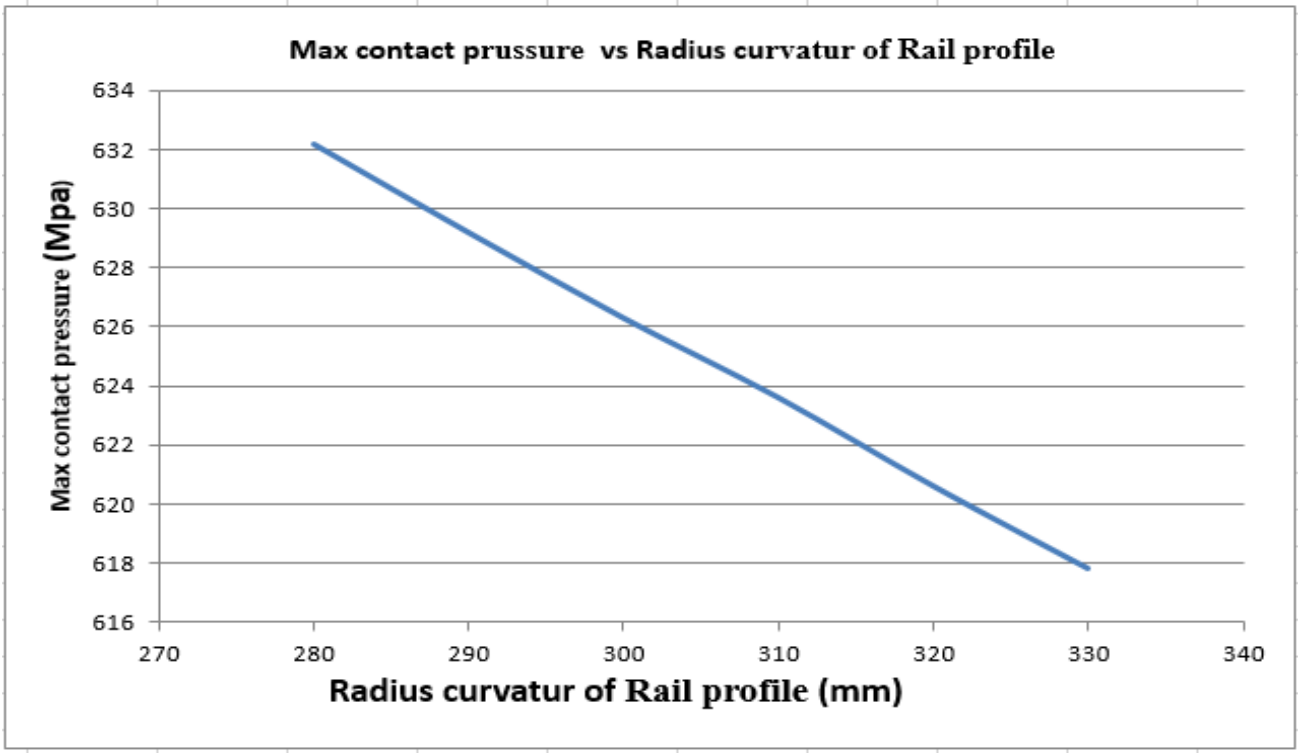


**Fig.4.4** Shows the reduction of contact pressure with the increase of radius curvature of rail profile

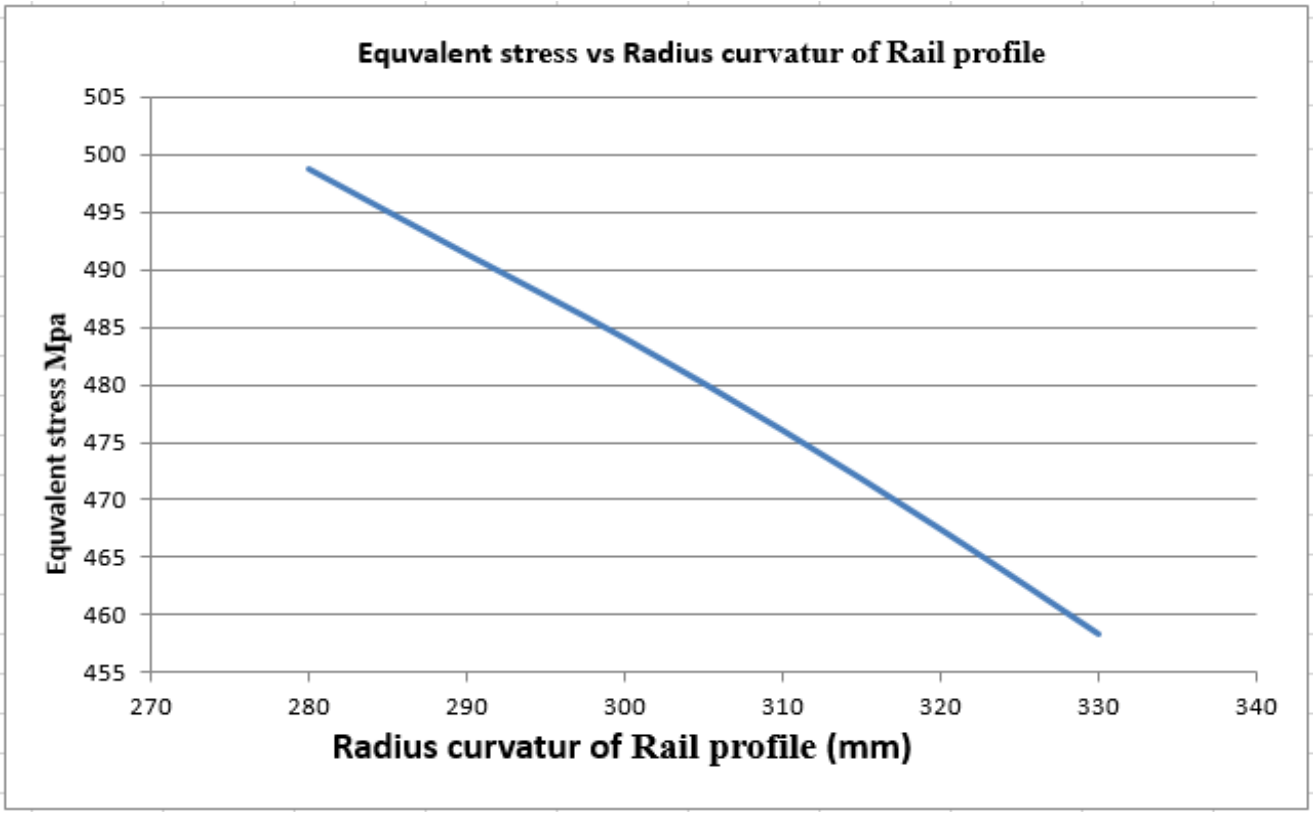


**Fig.4.5** Shows the reduction of equivalent stress with the increase of radius curvature of rail profile

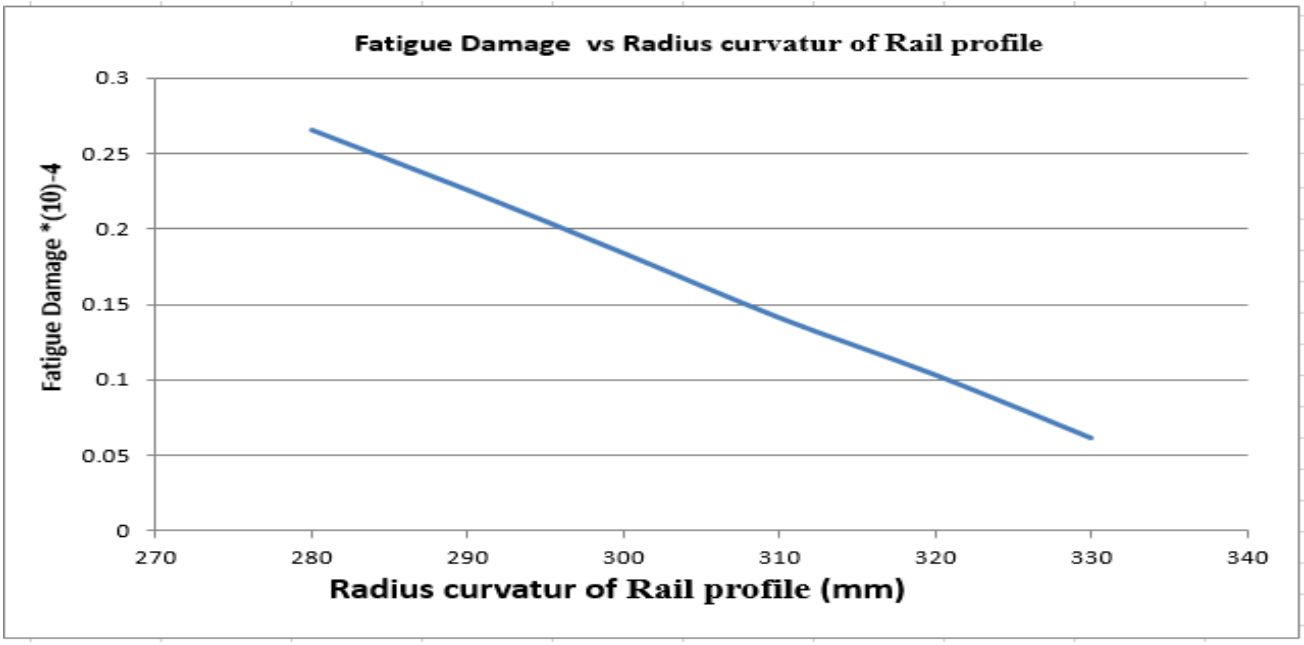


**Fig.4.6** Shows Reduction of fatigue damage with increase of radius curvature of rail profile

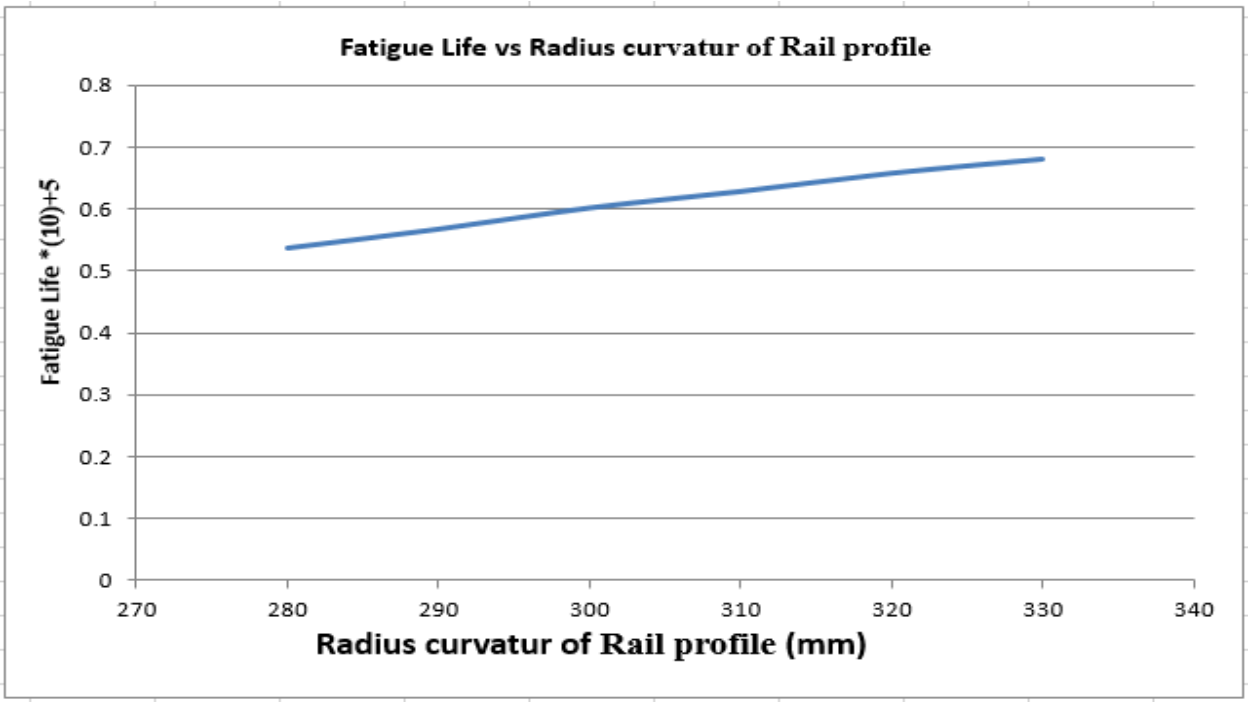


**Fig.4.7** Shows the increment of fatigue life with increase radius curvature of rail profile

## 4.3 Finite Element Results and Discussion

### 4.3.1 Modeling of Wheel / Rail Contact

A rail profile of UIC 60 and a wheel profile of S1002 are modeled using Catia V5R16 software as a separate part. The 3D geometric model of the wheel is generated by revolving the 3D curves that describe the profile of the wheel tread. The rail model is created by extruding railhead profile curves a distance of 600 mm, which is the distance between the sleepers. The two model parts are then assembled in catia workbench using constraints contact surface to surface assembly.

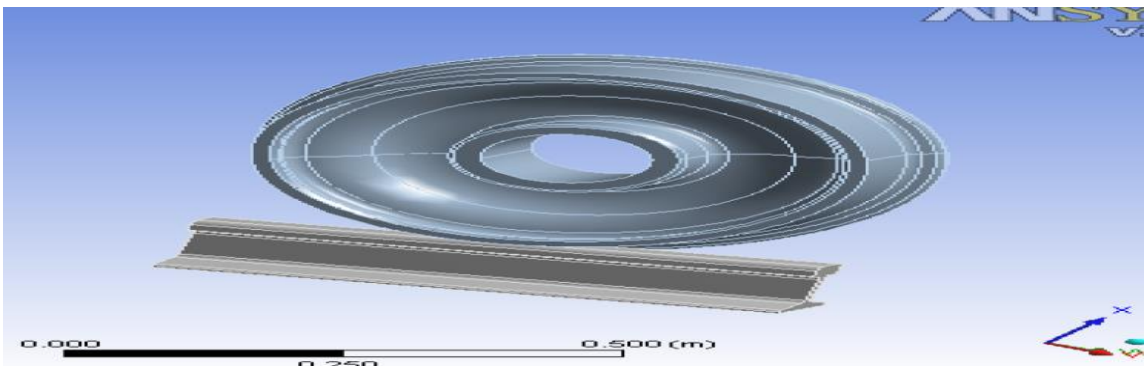


Figure **.4.8**: Wheel/rail contact model with CATIA V5

### 4.3.2 Meshing

The meshing used here is triangular surface meshing, and the size for meshing has been set up to the fine so that the accurate result may be achieved. Triangular meshing is the simplest one and easy to create and is being used in the structured grids. Fine meshing is preferred than coarse meshing as fine meshing is more robust and efficient to get the solution accurately.

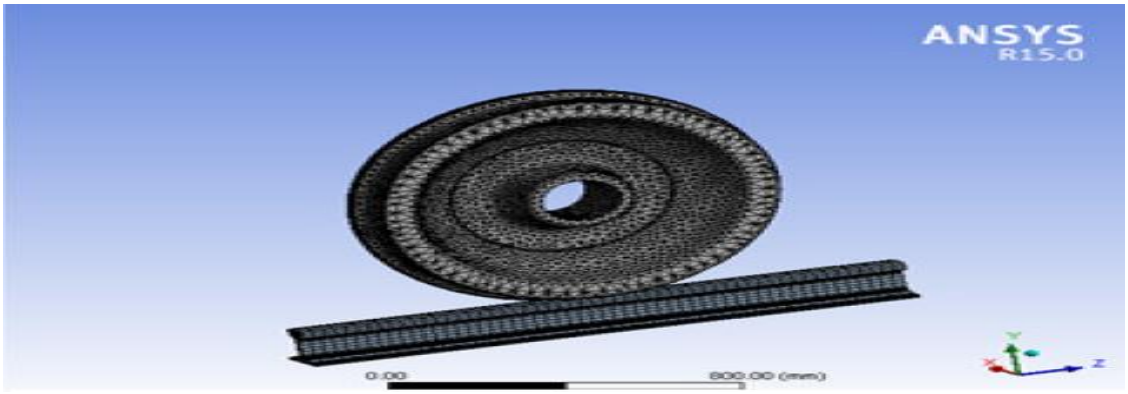


**Fig.4.9** meshed wheel-rail contact assembly in ANSYS.

## 4.4 Boundary Conditions

### 4.4.1 Fixed support

The analysis is of static structural type and requires fixing of the rail. So the fixed support has been provided to the rail by selecting the bottom face of the rail by enabling the faces election. This means that, fixed bottom face will not be translated or rotated in any of the directions.

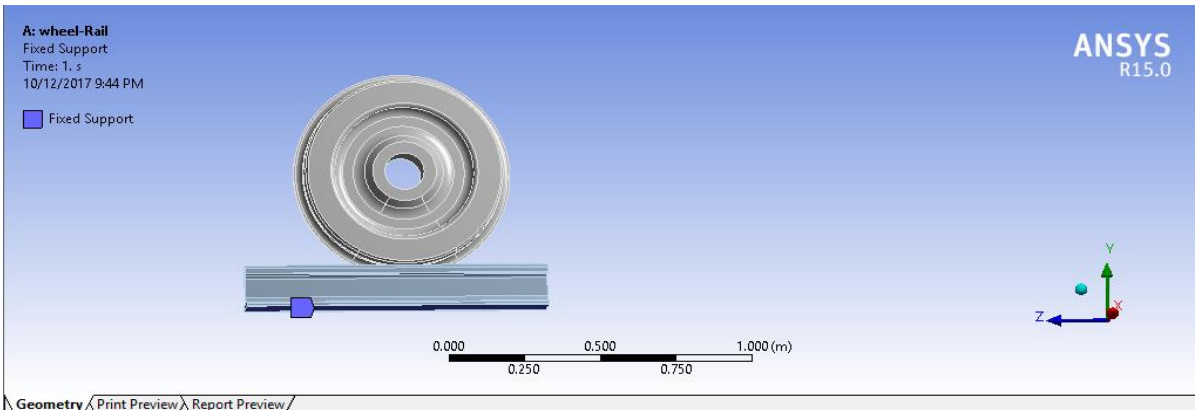


**Fig.4.10** Fixed boundary conditions of wheel rail contact assembly.

### 4.4.2 Force applied

The force will be applied in the negative direction so it has been taken in the vertical downward direction on the above face of Hub wheel. Hence, the force has been defined on the **y** component. The **y** component to be 53064.4N force. This force is half of the axle load as the axle load is divided into two parts for the two wheels i.e. maximum load which a wheel can take on UIC 50 kg rails.

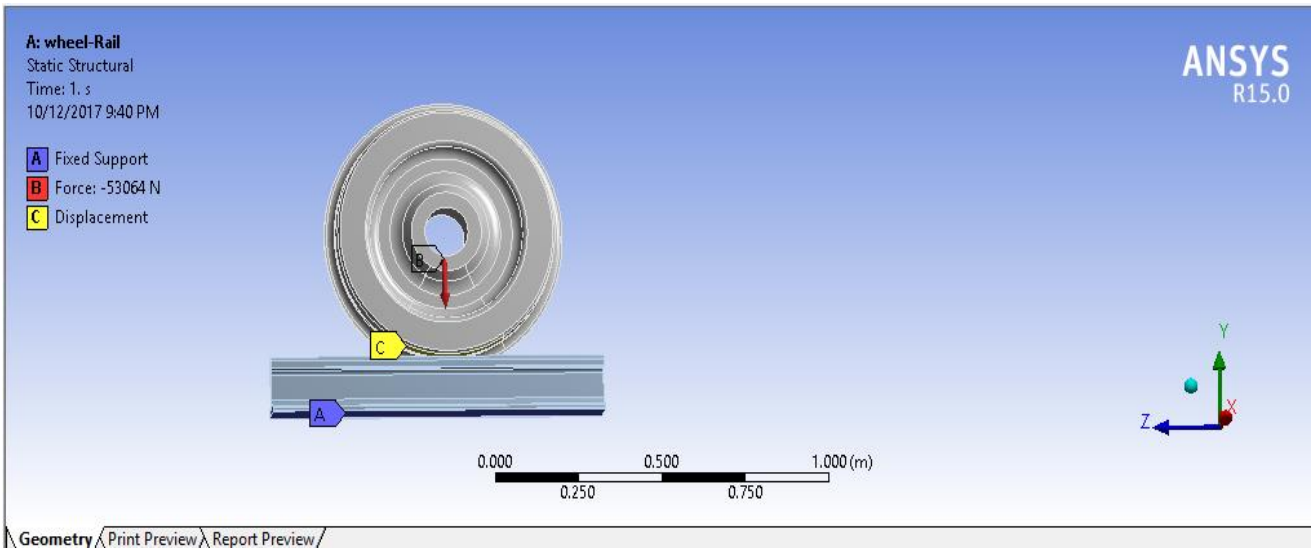


Fig.4.11 Force applied Boundary Conditions of vertical load for wheel rail contact assembly.

## 4.5. Equivalent stress (Von Misses Stress) Result

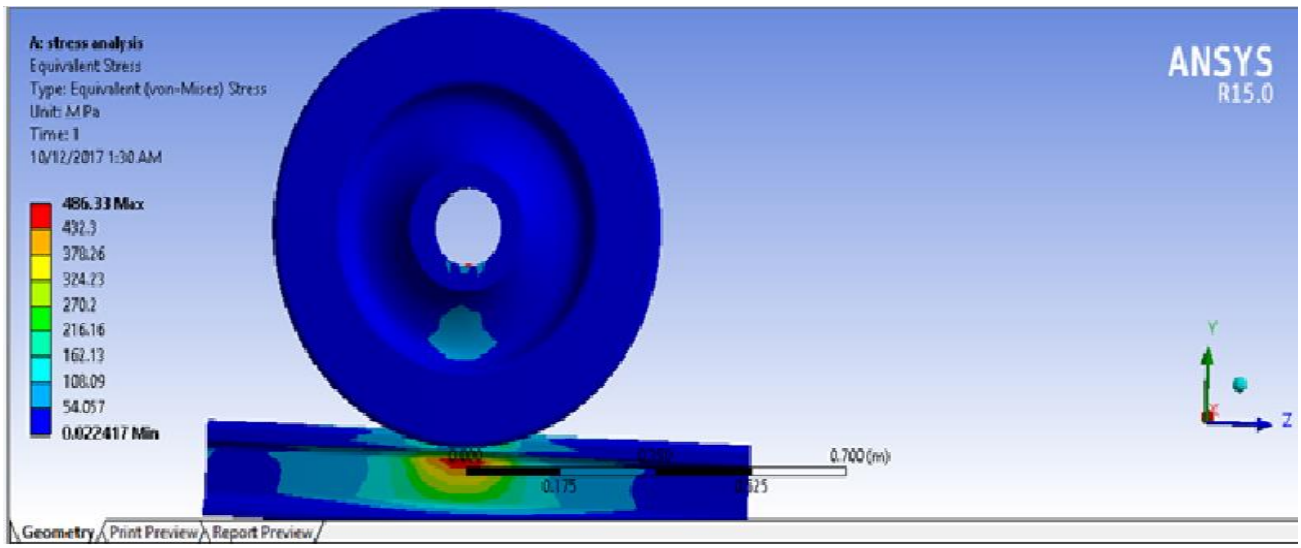


Fig.4.12 Equivalent stress Result for Radius curvature of Rail Profile 280mm

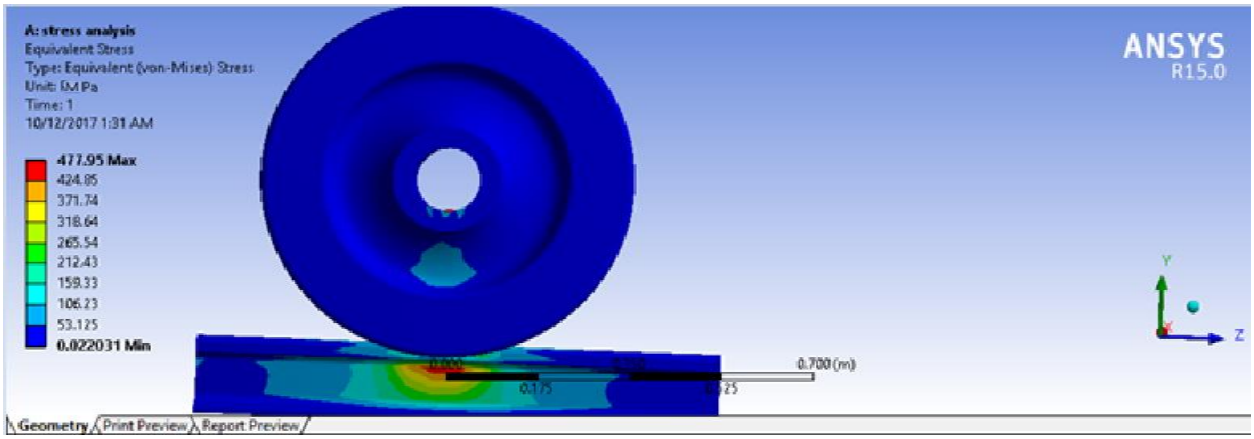


Fig.4.13 Equivalent stress Result for Radius curvature of Rail Profile 290mm

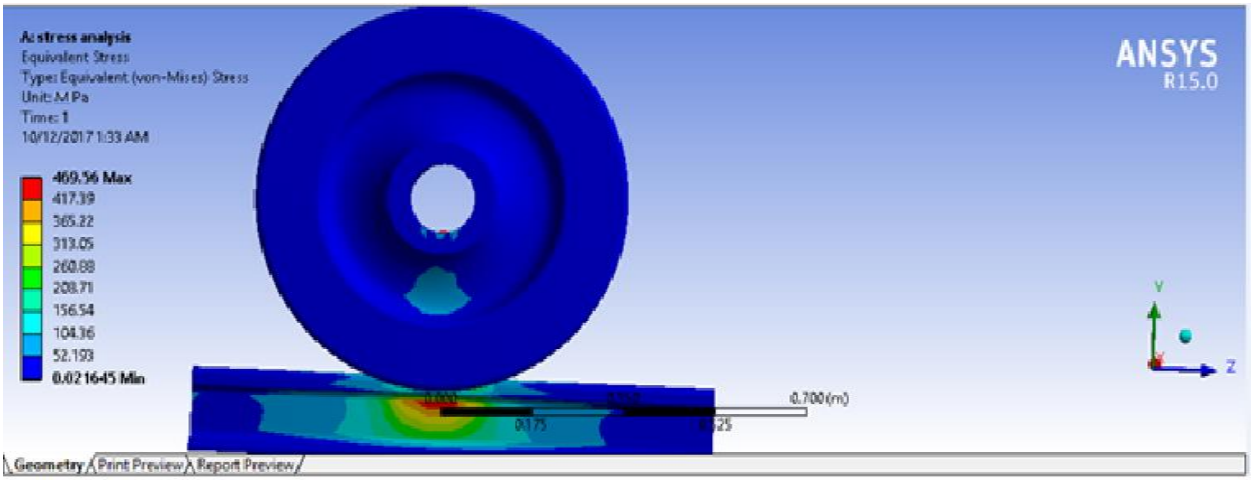


Fig.4.14 Equivalent stress Result for Radius curvature of Rail Profile 300mm

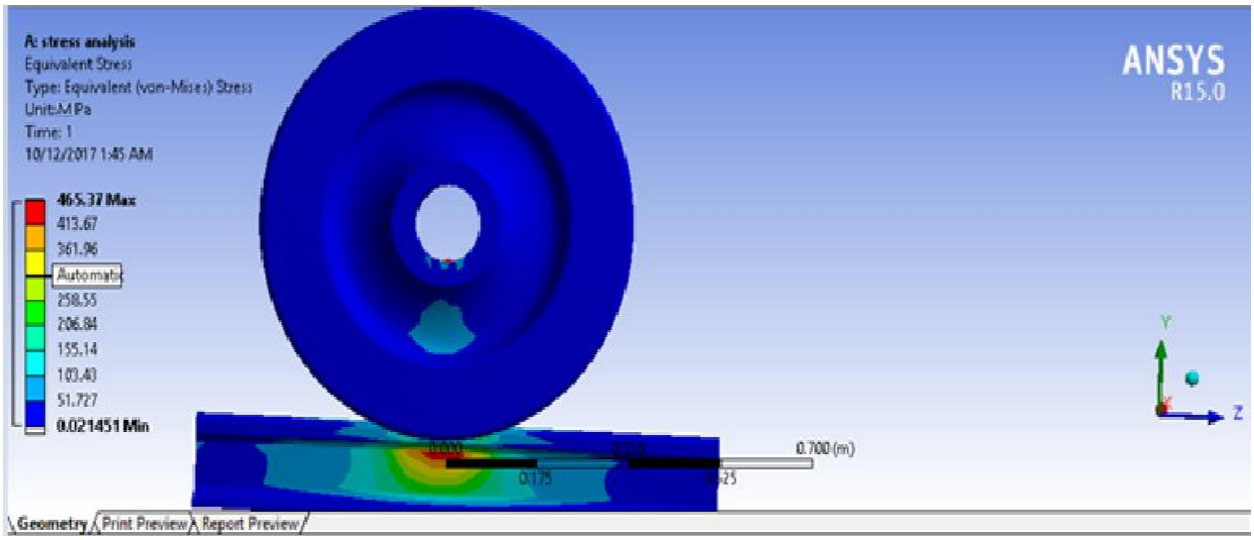


Fig.4.15 Equivalent stress Result for Radius curvature of Rail Profile 310mm

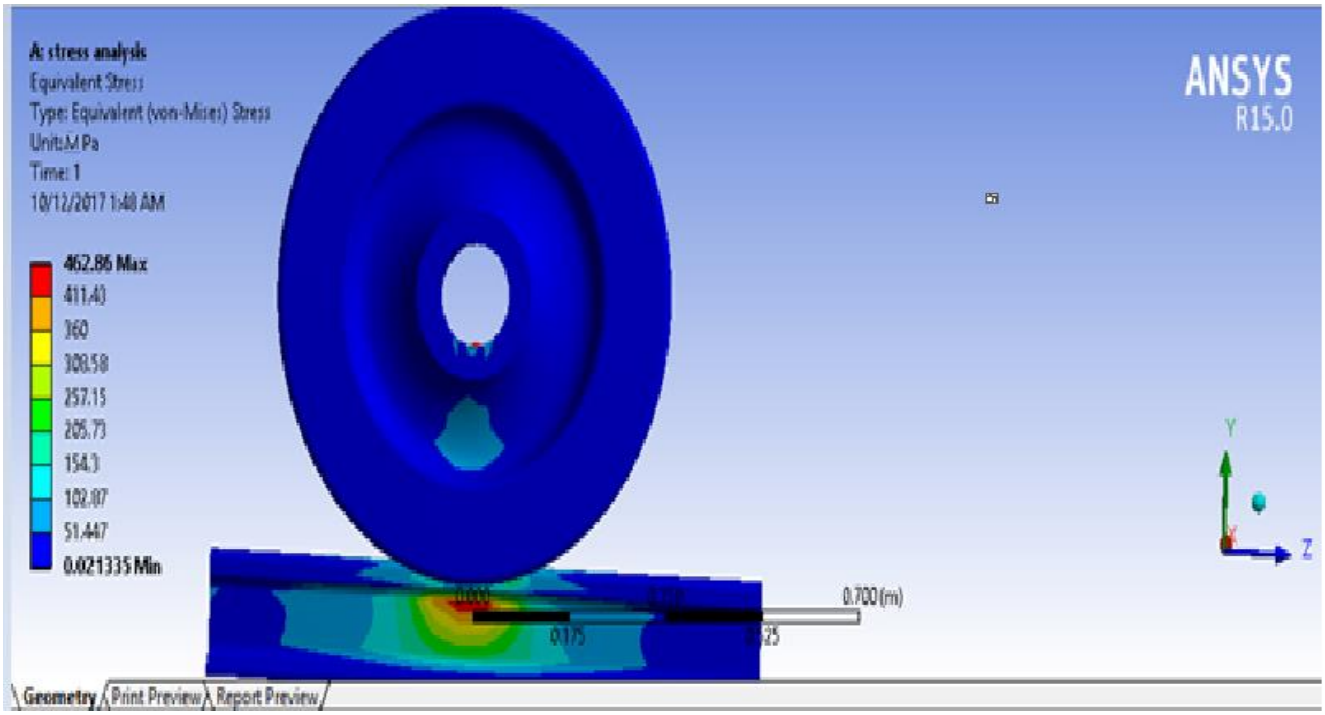


Fig.4.16 Equivalent stress Result for Radius curvature of Rail Profile 320mm

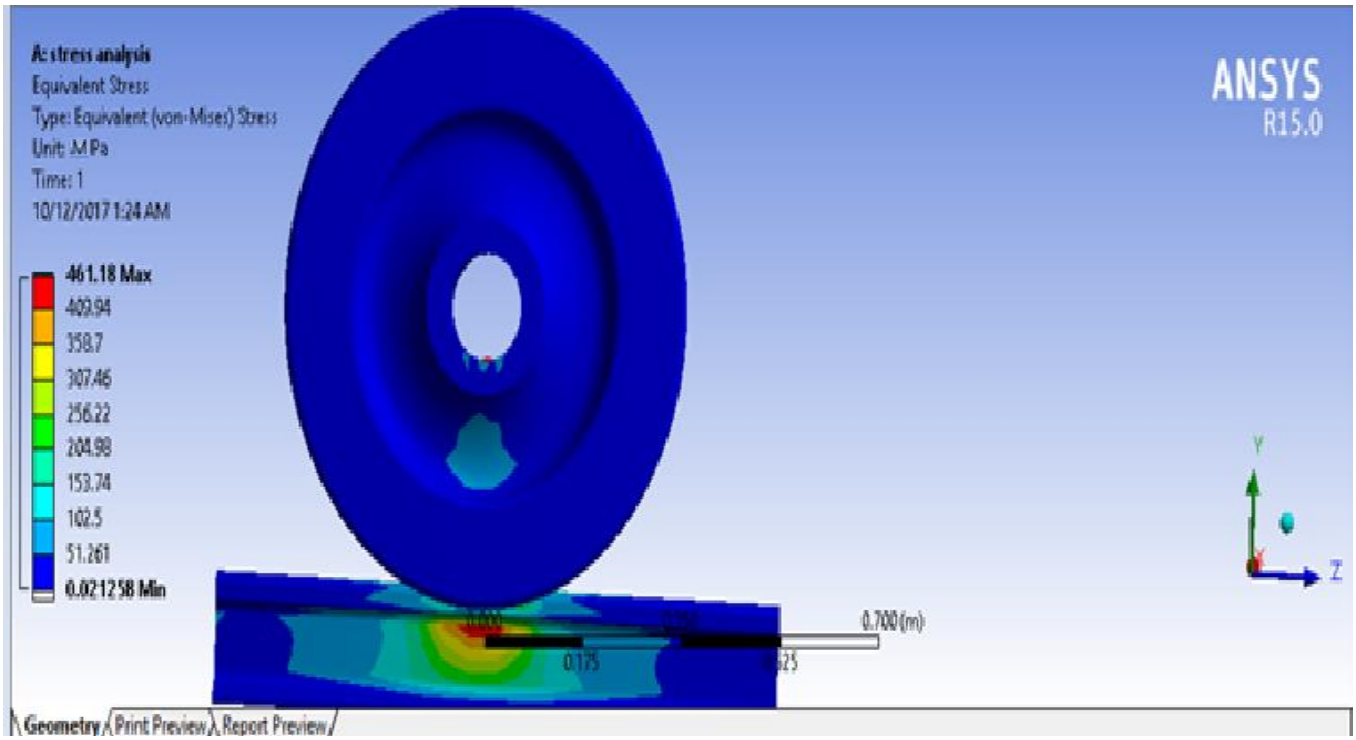


Fig.4.17 Equivalent stress Result for Radius curvature of Rail Profile 330mm

## 4.6. Fatigue life Result

This result contour plot shows us the available life for the given fatigue analysis. If loading is of constant amplitude, this represents the number of cycles until the part will fail due to fatigue

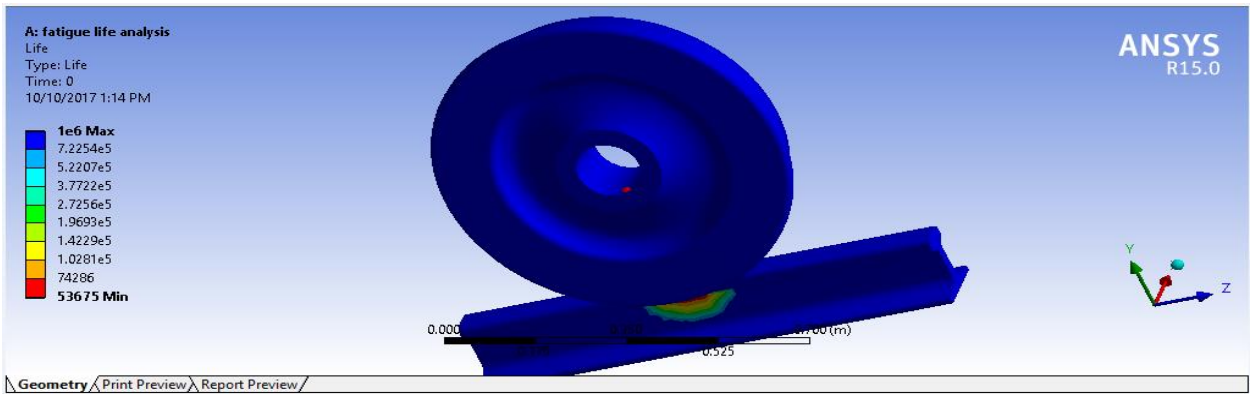


Fig.4.18 Fatigue life Result for Radius curvature of Rail Profile 280mm

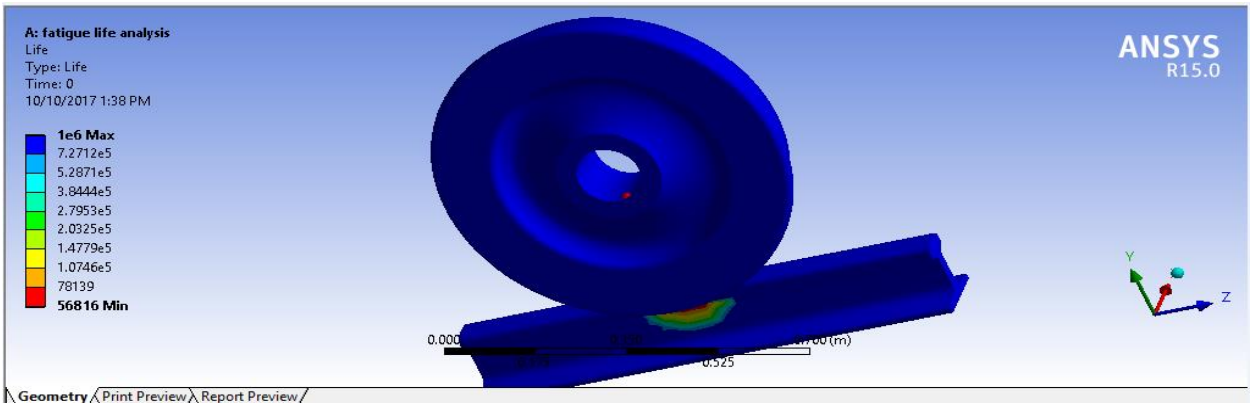


Fig.4.19 Fatigue life Result for Radius curvature of Rail Profile 290mm

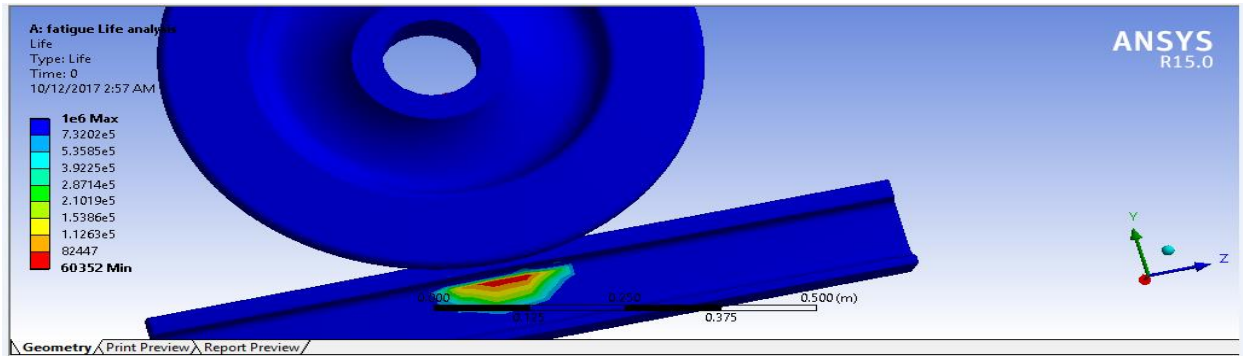


Fig.4.20 Fatigue life Result for Radius curvature of Rail Profile 300mm

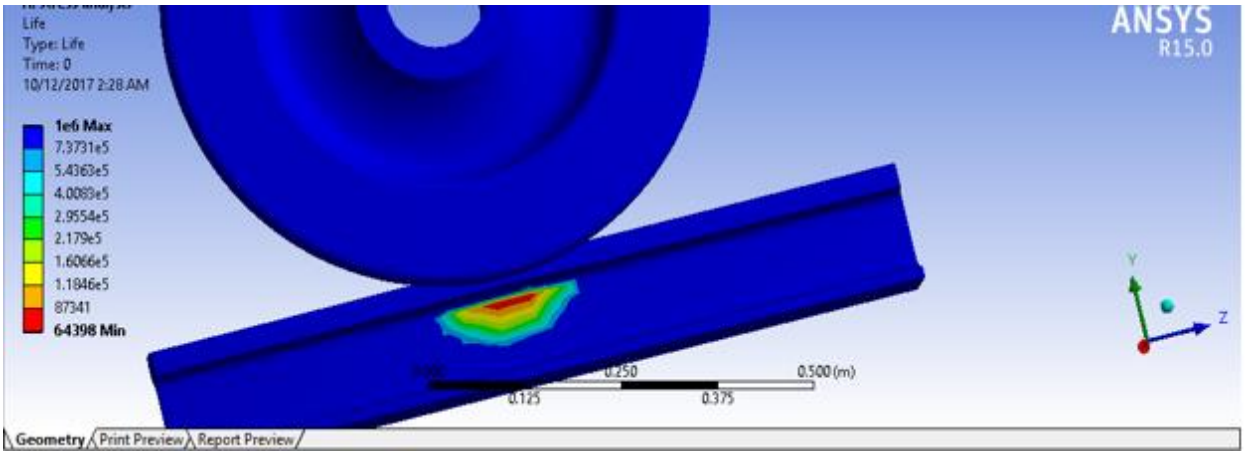


Fig.4.2.1 Fatigue life Result for Radius curvature of Rail Profile 310mm

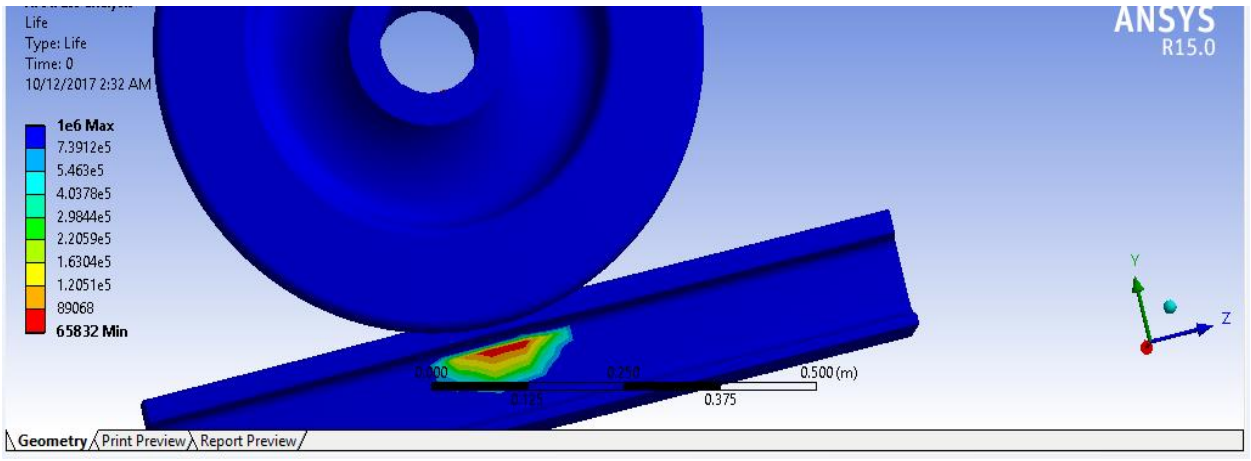


Fig.4.2.2 Fatigue life Result for Radius curvature of Rail Profile 320mm

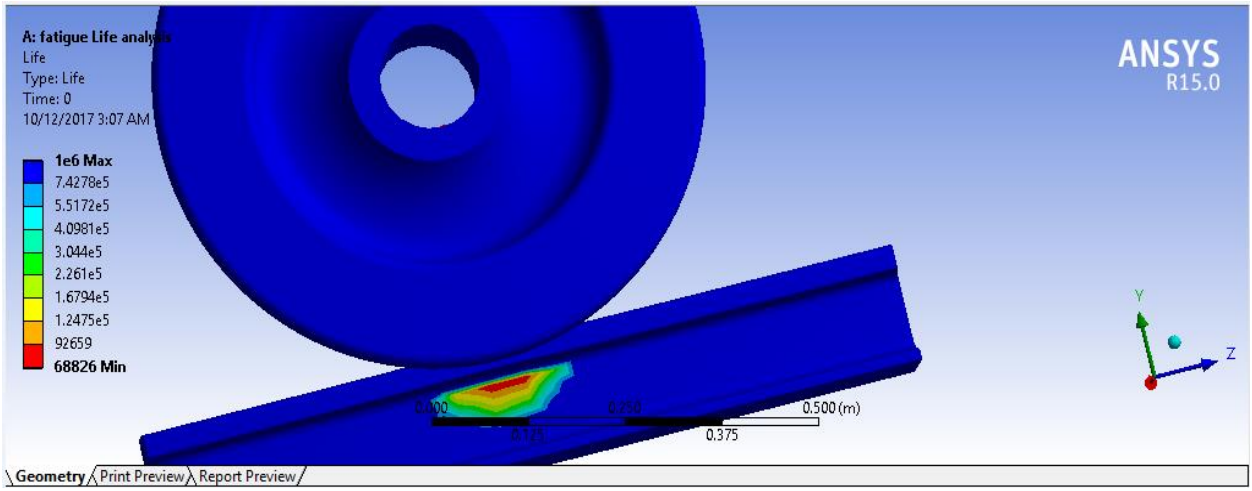


Fig.4.2.3 Fatigue life Result for Radius curvature of Rail Profile 330mm

**Table 4.2**: Comparison of the theoretical and finite element results of expected stress fatigue life for variable radius of curvatures of rail profiles.

| Transversal radius of curvature of rail profile (mm) at the contact point | Theoretical(analytical )results of the available fatigue life | ANSYS workbench results of the available fatigue life | Error in percent, (%) |
|---|---|---|---|
| 280 | 5.3763 | 53675 | 0.14 |
| 290 | 5.6818 | 56816 | 0.23 |
| 300 | 6.0241 | 60352 | 1.79 |
| 310 | 6.2893 | 64398 | 2.39 |
| 320 | 6.5835 | 65832 | 1.38 |
| 330 | 6.8114 | 68826 | 2.55 |

**Table 4.3**: Comparison of the theoretical and finite element results of Von Mises (equivalent) stress for variable radius of curvatures of rail profiles.

| Transversal radius of curvature of rail profile (mm) at the contact point | Theoretical (analytical) results of the Von Misses (equivalent) stress. (MPa) | ANSYS workbench results of the Von Misses (equivalent stress.(MPa) | Error in percent, (%) |
|---|---|---|---|
| 280 | 498.8 | 486.33 | 1.54 |
| 290 | 491.4 | 477.95 | 1.18 |
| 300 | 484.1 | 469.56 | 0.45 |
| 310 | 476.2 | 465.37 | 0.41 |
| 320 | 467.5 | 462.86 | 0.29 |
| 330 | 458.4 | 461.18 | 0.61 |

Therefore, as shown in table (4.2) and table (4.3) the ANSYS workbench indicates comparable results as that of the theoretical one.

# Chapter Five

# Conclusion Recommendation and future works

## 5.1. Conclusion

Rail- wheel contact problem varying in radiuses curvature of rail profile is investigated to estimate the influence of contact area and stress distribution. Results from the present model indicate Elliptical contact dimensions (major 'a' and Mainor axis 'b') contact area (πab) and fatigue life increase when the radius curvature of Rail Profile is increased and the maximum contact pressure, principal stress, equivalent stress, fatigue damage will decrease when the Rail Profile is increased. On the other hand, higher radius of curvature for rail profiles promotes a reduction on rolling contact fatigue For instance, if Japanize industrial standard JIS 37kg and Russian Standard GOST P 60KG A rails with radius of curvature R=304.80mm and are R=330 respectively compared to Chinese national railway standard GB 50kg rail , with radius of curvature R=300mm ,which is operational for Addis Ababa Light Rail Train, a slight increment of radius of curvature of 4.80mm and 30mm can be deduced from the rail profiles at the contact region .Under the same vehicle specification ,this slight variation of radius of curvature generates an increase in contact area of magnitude 0.30576mm2 and 2.65mm$^2$ which is responsible for a reduction in the maximum contact pressure of 5.14MPa and 6.5MPa consequently an increase in expected fatigue life of 2493.6 cycles and 6874 cycles. Other standard rail profiles such as Japanese Industrial Standard JIS 60kg (radius of curvature 600mm) and Russian Standard GOST P 65kg (radius of curvature 500mm) has an enormous reduction in wheel fatigue damage compared to Chinese GB 50kg standard rails and possesses significantly better fatigue life.

The present analysis may help in rail wheel profile design keeping care of, contact stress, contact pressure and vehicle stability for optimization of wheel and rail profiles. Obviously, better wheel rail performance can be achieved compromising all these elements.

## 5.2. Recommendation

As long as the target is to decrease rolling contact fatigue phenomenon, higher radius of curvature for rail profiles is recommendable.
Use of large Radius curvatures of rail profiles significantly reduces contact fatigue stresses

It should be noted that, since rail profiles cannot be changed instantaneously, the transition from current to new shapes must be properly considered during profile design

## 5.3. Future works

On the present study wheel rail contact is taken into consideration at the wheel tread rail head contact which is mainly a contact zone on a straight track. Hertzman contact assumptions can be applicable in these zones. However, on curves of a track contact will be shifted from wheel tread rail head to wheel flange rail gauge corner. Hertzman theories cannot be applied in these zones because one of the assumptions of Hertzman theory is to take large curvature radius compared to the contact size. However, the radii of curvatures in these zones are very small and Hertzman assumption will be inaccurate. Only finite element approaches can give us a better solution. Future researchers are expected to investigate what rolling contact fatigue is like for effect of changes of rail profiles in these zones. The predictions of rolling contact fatigue in this thesis reflect the exponential growth of the fatigue damage based on the Dang Van equivalent stress. It simply predicts general fatigue damage based on stress. It does not identify crack initiation and crack propagation.

This investigation considers static contact condition to future study of their dynamic behavior.

## Reference

1. CRN RS 006: Minimum Operating Requirements For Road Rail Infrastructure Maintenance Vehicles: Version1.0 Issued December 2011,Principal Rolling Stock Engineer,USA 2011.

2. Iwnicki S. (ed.), (2006) Handbook of railway vehicle dynamics, CRC Press, Taylor & Francis Group, 2006, ISBN-13: 978-0-8493-3321-7.

3. Ivan Y. Shevtsov: Wheel/Rail Interface Optimization ,Section of Road and Railway Engineering Faculty of Civil Engineering and Geosciences, Delft University of Technology Delft, Netherlands, 2008

4. Branislav Sladojevic, Milos Jelic, Milica Puzic: New Requirements for The Quality Of Steel Rails, 4th International Conference Processing and Structure Of Materials Held On Palic, Serbia May 27- 29, 2010

5. Tanel Telliskivi: Wheel-Rail Interaction Analysis, Department of Machine Design Royal Institute of Technology, Kth Se – 100 44 Stockholm, Sweden, 2003

6. Gunter Schupp , Christoph Weidemann And Lutz Mauer, 2007,Modeling The Contact Between Wheel And Rail Within Multibody System Simulation German Aerospace Center, Institute Of Aero Elasticity, Germany

7. Ulf Olofsson and Roger Lewis: Hand book of rail way vehicle dynamics, Tribology of the Wheel – Rail Contact, Taylor & Francis Group, LLC , pp.121-138,2006

8. Eric Magel, Peter Sroba, Kevin Sawley and Joe Kalousek : Control of Rolling Contact Fatigue of Rails ,Centre for Surface Transportation Technology, National Research Council ,Canada

9 Pislaru, Crinela (2012) :Modelling and Simulation of the Dynamic Behaviour of Wheel-Rail Interface, In: IET Event: The Railway Wheel-Rail Interface: Damage Mechanisms and Potential Solutions, 5 March 2012, University of Huddersfield .

10. Gunter Schupp , Christoph Weidemann And Lutz Mauer, 2007,Modeling The Contact Between Wheel And Rail Within Multibody System Simulation German Aerospace Center, Institute Of Aero Elasticity, Germany

11. Paul Boyd, Manicka Dhanasekar: Wheel / Rail Contact Analysis
Central Queensland University, Centre for Railway Engineering, Qld 4702, Australia, 2002

12 Marine Vidaud, Dr. Willem-Jan Zwanenburg : Current situation on rolling contact fatigue – a rail wear phenomenon, Swiss Transport Research Conference , Monte Verita /Ascona ,*Sept 9* - 13.

F. Carter, On the action of a locomotive driving wheel, Proc. R. Soc. London 112 (1926)

14. K. Johnson, Contact Mechanics, Cambridge University Press, Cambridge, 1985.

15. J. Kalker, Three-Dimensional Elastic Bodies in Rolling Contact, Kluwer Academis Publishers, Dordrecht, 1990.

16 P. Wriggers, Computational contact mechanics, John Wiley & Sons Ltd., Chichester, 2002.

17. Matin Shahzamanian Sichani: Wheel-Rail Contact Modelling in Vehicle Dynamics Simulation, KTH Engineering Sciences, Licentiate Thesis Stockholm, Sweden 2013

18. Kapok, A (1994), Re-evaluation of the life to rupture of ductile metals by cyclic plastic strain, Fatigue & Fracture of Engineering Materials & Structures, 17(2), 201-19.

19. Kabo, E., Ekberg, A., 2005. Material defects in rolling contact fatigue of railway wheels – the influence of defect size. Wear 258 (7–8), 1194–1200.

20. Kabo, E., 2002. Material defects in rolling contact fatigue of railway wheels – influence of overloads and defect clusters. International Journal of Fatigue 24 (8), 887–894.

21. Hrennikoff, Alexander (1941) "Solution of problems of elasticity by the framework method".

22. Kabob, E., 2002. Material defects in rolling contact fatigue of railway wheels – influence of overloads and defect clusters. International Journal of Fatigue 24 (8), 887–894.*Journal of applied mechanics* **8.4**: 169–175.)

23. Kabo, E., Ekberg, A., 2005. Material defects in rolling contact fatigue of railway wheels – the influence of defect size. Wear 258 (7–8), 1194–1200.

24. Michael G/mariam, Effect of Change of Contact Ratio on Contact Fatigue Stress of Spur Gears: Addis Ababa University School Of Graduate Studies, Addis Ababa, 2013